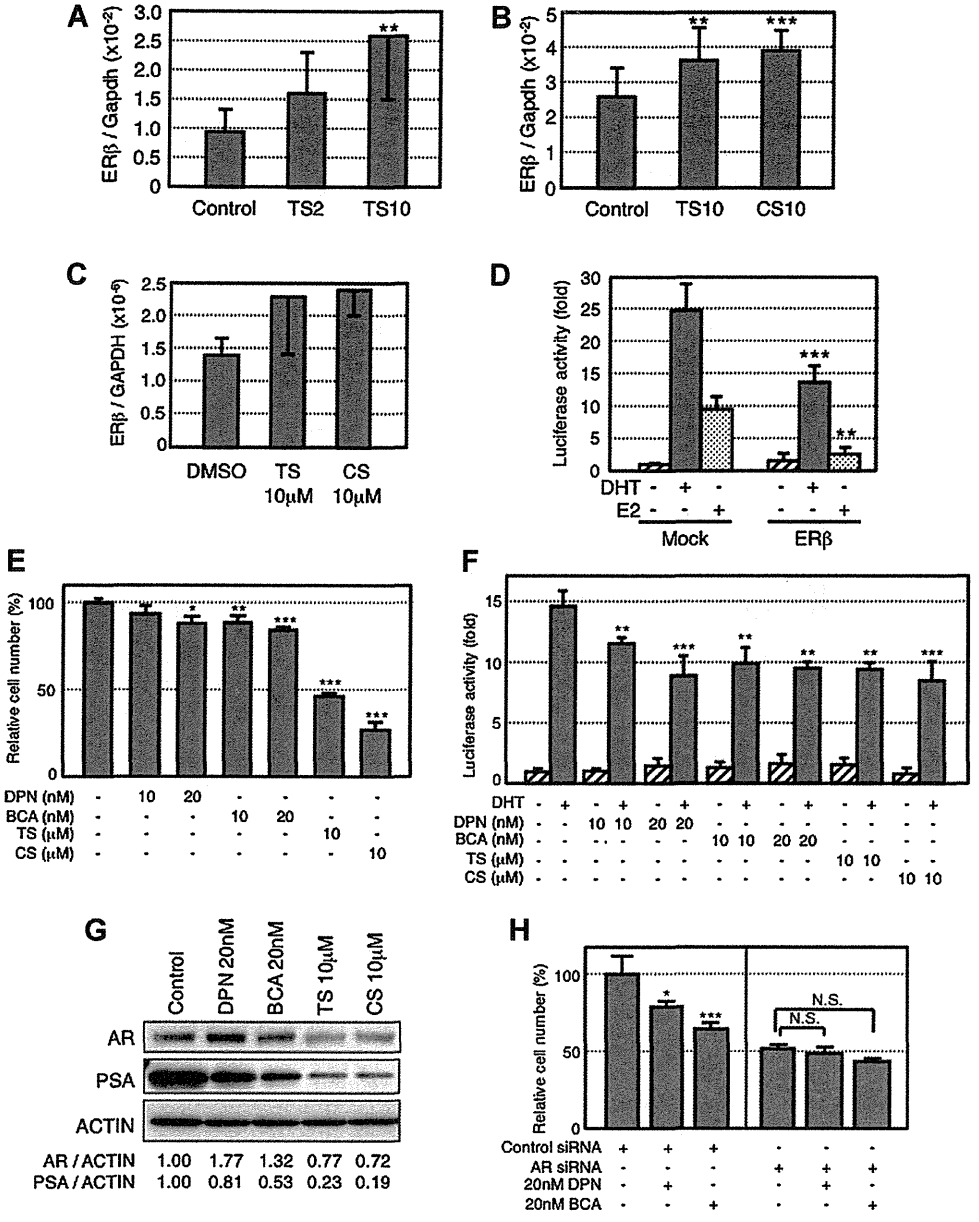

Fig. 3. Effects of ARBs on ERβ mRNA expression in TRAP rats or LNCaP cells. Real-time-RT-PCR for ERβ in ventral prostate of TRAP rats from Experiment I (**A**) and from Experiment 2 (**B**) Data in (A) and (B) were analyzed using all animal samples. **C**: Real-time RT-PCR for ERβ using total RNA of LNCaP cells treated with ARBs for 3 days. **D**: Inhibition of PSA promoter luciferase activity by ERβ in LNCaP cells. Cells were transfected with pGL3/PSA promoter, phRL-TK Renilla luciferase vector and expression plasmid encoding human ERβ (pCXN2/ERβ) or mock vector (pCXN2). Cells were incubated in the absence or presence of 5 nM DHT or 100 nM 17β-estradiol (E2) for 48 hr. Data represent the mean and standard deviation of four independent data points. **E**: Cell growth after chemical exposure of ARBs or selective ERβ agonist in LNCaP. Cells were exposed to chemicals for 72 hr, and cell growth was evaluated by WST-1 assay. **F**: Inhibition of PSA promoter luciferase activity by ARBs or selective ERβ agonist in LNCaP cells. Cells were transfected with the same as (D). Cells were treated in the absence or presence of 5 nM DHT and/or ARBs or a selective ERβ agonist as indicated for 48 hr in RPMI1640 containing 10% charcoal-stripped FBS without phenol red. Data represent the mean and standard deviation of four independent data points. **G**: Immunoblots of protein lysates of LNCaP exposed ARBs or selective ERβ agonist for 3 days. The intensity of each band was measured and normalized to actin. **H**: LNCaP cells were transfected with either control siRNA or AR siRNA and then were exposed to selective ERβ agonists 1 day after transfection. Cells were incubated with RPMI1640 containing 5% FBS without phenol red for 3 days. Cell growth was evaluated by WST-1 assay. N.S., not significant. TS2 and TS10, telmisartan 2 and 10 mg/kg/day, respectively; CS10, candesartan 10 mg/kg/day; DPN, diarylpropionitrile; BCA, biochanin A. $^{*,***}P < 0.05$ and 0.001 versus control, respectively.

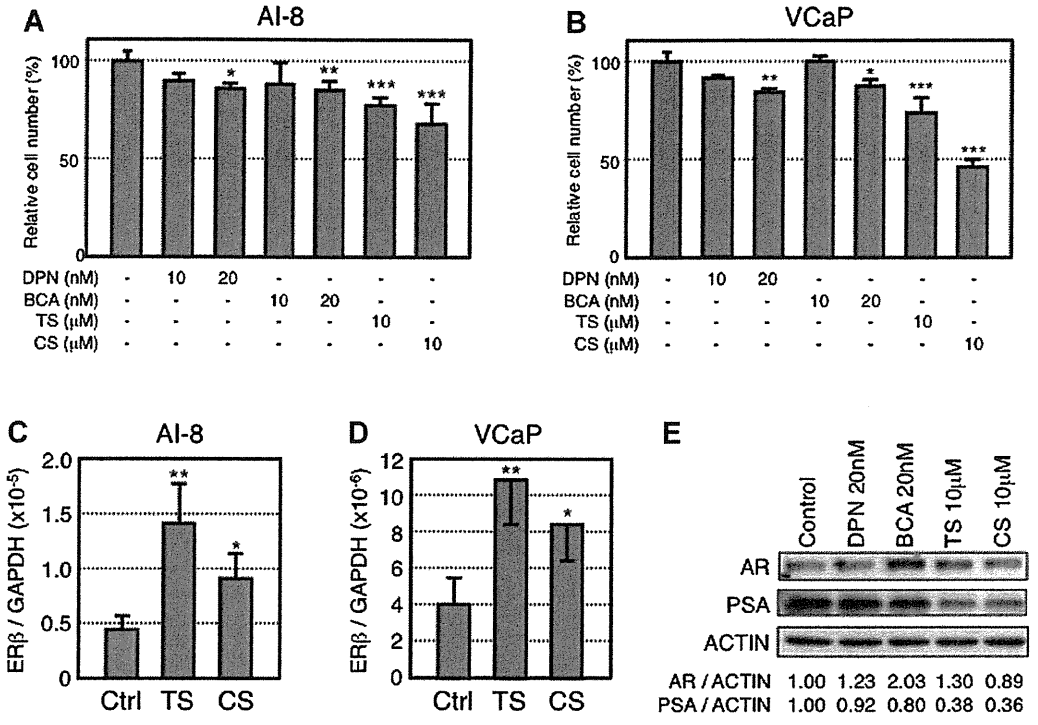

Fig. 4. Effects of ARBs or selective ERβ agonist on the growth, expression of AR, PSA, and ERβ in androgen-independent human prostate cancer cell lines, LNCaP subline, AI-8, and VCaP. AI-8 was incubated in RPMI1640 containing 10% charcoal-stripped FBS and 5 nM DHT without phenol red and VCaP was incubated in RPMI1640 containing 10% FBS with phenol red. AI-8 (**A**) and VCaP (**B**) cells were exposed to chemicals for 72 hr, and cell growth was evaluated by WST-1 assay. The mean values of six independent data points are presented and SD values are indicated by bars. $^{*},^{**},^{***}P < 0.05$, 0.01, and 0.001 versus control, respectively. (**C**,**D**) Real-time RT-PCR for ERβ using total RNA of AI-8 (C) and VCaP (D) exposed 10 μM TS or CS for 3 days. GAPDH gene was used as an internal control. The data represent the mean ± SD. $^{*},^{**}P < 0.05$ and 0.01 versus control, respectively. **E**: Immunoblots of protein lysates (20 μg) of AI-8 exposed ARBs or selective ERβ agonist for 3 days were probed with antibodies to AR, PSA, and β-actin. The intensity of each band was measured and normalized to actin. DPN, diarylpropionitrile; BCA, biochanin A; TS, telmisartan; CS, candesartan; Ctrl, control.

proliferation, suggesting the role of ERβ was a mild additional modifier on AR-mediated transcriptional activity (Fig. S7). To examine the effect of ARBs on the growth of androgen-independent LNCaP cells, we used VCaP and AI-8 cells, which possessed the highest PSA expression among the four sublines (Fig. S1C). Selective ERβ agonists as well as ARBs inhibited cell proliferation of both AI-8 and VCaP cells (Fig. 4A,B). Immunoblot analysis revealed that AR expression was increased while PSA was decreased by treatment with selective ERβ agonists in AI-8 cells (Fig. 4E). On the other hand, ARBs clearly repressed PSA expression although the AR protein level was slight increased with telmisartan (TS) and decreased with candesartan (CS) treatment compared with the no-treatment control. These results are in marked contrast to the findings seen in androgen-dependent parental LNCaP cells as shown in Fig. 3G. Up-regulation of ERβ mRNA expression by ARB treatment was observed in both AI-8 and VCaP cell (Fig. 4C,D).

Intervention Study

Background data of the patients are shown in Table S7. aPSA-DT was significantly longer than ePSA-DT in both the olmesartan-treated patients (see Materials and Methods Section), median 436.3 versus 128.7 days ($P = 0.004$; Fig. 5A). However, the ratio of aPSA-DT/ePSA-DT was significantly longer in olmesartan-treated patients (3.36 times) than in control patients (1.80 times) ($P = 0.0156$), indicating that olmesartan treatment could delay PSA progression (Fig. 5B). Fig. 5C shows that $TTPP_{1.0}$ from biochemical failure (0.2 ng/ml) to over 1.0 ng/ml in olmesartan-treated patients was significantly longer than that in control patients (no treatment; $P = 0.026$). Similarly, the time for PSA progression from the PSA nadir to over

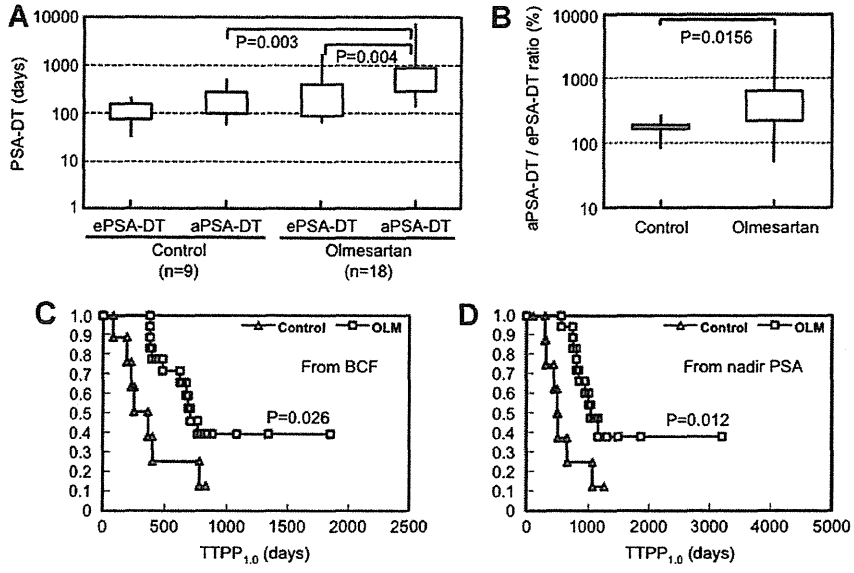

Fig. 5. PSA-DT in control and olmesartan-treated patients. **A**: ePSA-DT and aPSA-DT in control and olmesartan-treated patients. aPSA-DT was significantly longer than ePSA-DTs in olmesartan-treated patients ($P = 0.004$) or aPSA-DT in control patients ($P = 0.003$). **B**: The ratio of aPSA-DT/ePSA-DT was significantly higher in olmesartan-treated patients (3.36 times) than in control patients (1.80 times) ($P = 0.0156$). Kaplan–Meier plots illustrating time to PSA progression in control and olmesartan (OLM)-treated patients. **C**: Time to PSA progression from biochemical failure (0.2 ng/ml) to over 1.0 ng/ml in olmesartan treated patients was significantly longer than that in control patients ($P = 0.026$). **D**: Time to PSA progression from PSA nadir to over 1.0 ng/ml in olmesartan-treated patients was significantly longer than that in control patients ($P = 0.012$). BCF, biochemical failure.

1.0 ng/ml in olmesartan-treated patients was significantly longer than that in control patients ($P = 0.012$) as shown in Fig. 5D.

DISCUSSION

It is widely accepted that there are multiple processes in the development of cancer; that is, initiation, promotion and progression. In 1976, Sporn proposed "cancer chemoprevention" as a strategy for prevention of cancer to delay the development of clinically evident disease by suppression of progression from precancerous lesions to invasive cancer by giving natural or synthetic compounds [17]. Prostate cancer is known to be strongly associated with aging, that is, about three-quarters of cases worldwide occur in men aged 65 years or more [18]. Therefore, prostate cancer is an attractive target for cancer chemoprevention because of the high population incidence and long latent period, and several dietary factors as well as genetic background have been linked to risk and progression of prostate cancer [19,20]. In fact, a large number of observational or intervention studies have been conducted using vitamins, phytochemicals, and minerals [21,22]. Moreover, three large scale randomized clinical trials, SELECT (Selenium and Vitamin E Cancer Prevention Trial) [23], PCPT (Prostate Cancer Prevention Trial) [24], and REDUCE (Reduction by Dutasteride of Prostate Cancer Events) [25], have been completed, and the latter two trials using 5α-reductase inhibitors showed a reduction of prostate cancer risk, although adverse effects including sexual dysfunction were observed. From the viewpoint of sexual dysfunction, ARB could restore rather than induce these side effects [26–28].

The present study demonstrated suppressive effects of ARBs on prostate tumor progression in an in vivo animal model, with decrease in the development of both HG-PINs and adenocarcinoma and consequent increase in LG-PINs in the ventral prostate. We have validated the chemopreventive effects of various chemicals including anti-androgens using our TRAP rats [14,15,29,30]. This transgenic rat is characterized by the sequential development of prostatic lesions, that is, LG-PINs, HG-PINs and adenocarcinomas in almost all acini in the entire ventral and lateral lobes. The SV40 T antigen used in the transgene of the TRAP rat acts as a potent oncoprotein to strongly stimulate cell growth and the development of adenocarcinomas in almost all acini in the entire prostatic lobes through inhibiting both the pRB and p53 tumor suppressor pathways. Since expression of SV40 T antigen is regulated by the androgen-dependent probasin promoter, it is speculated that cancer

development in TRAP rats is very sensitive to chemicals that modulate the AR axis, including the endogenous androgen level. The possibility that suppressive effects of ARBs were due to down-regulation of the transgene expression could be excluded by the data on SV40 T antigen expression shown in Figures 2A and S4A. The in vivo finding that ARBs not only down-regulated AR protein but also suppressed the androgen responsive gene, GK11, an ortholog of human PSA, at the mRNA level, provided evidence that ARBs functionally suppressed the AR pathway in prostatic lesions of TRAP rats. Thus, the present study highlighted that the main pathway responsible for attenuation of prostate carcinogenesis by ARBs is the AR signal pathway through suppression of AR-mediated transcriptional activity by both AR down-regulation and ERβ up-regulation, as well as inactivation of the p38 MAPK pathway.

ERβ is known to regulate prostate gland growth as an antiproliferative receptor [31]. This study demonstrated that ERβ is one of the downstream molecules of AT1R, and the ERβ signal transduction pathway plays an important role in the mechanisms of suppression of prostate carcinogenesis by ARBs. Genistein and deizein, major components of soybean isoflavone, have been shown to exert suppressive effects on rat prostate carcinogenesis [32], and these compounds are known to bind ERβ and to have ERβ agonistic activity [33]. Gamma-tocopherol has also demonstrated an inhibitory effect on prostate carcinogenesis in TRAP rats by activation of caspase signaling [15] and it is speculated that the ERβ signal pathway might be involved in these inhibitory effects because gamma-tocotrienol was recently revealed to induce apoptosis by activation of caspase 3 and ERβ signaling [34]. The latest report suggests that ERβ exerts a pivotal role in sustaining the epithelial phenotype and suppressing the acquisition of epithelial-mesenchymal transition and aggressive characteristics of prostate cancer [35]. This accumulating evidence suggests that modulators of ERβ might be potential chemopreventive or chemotherapeutic agents.

Among the ARBs used here, telmisartan demonstrated PPARγ activation while candesartan and olmesartan did not [36]. Additionally, olmesartan is known to increase angiotensin 1–7 levels through activation of angiotensin converting enzyme 2 [37]. No toxic effects were observed in TRAP rats treated with candesartan while significant suppression of body weight gain was found with the high-dose telmisartan. These phenomena are presumably PPARγ-related and similar effects of telmisartan have been reported previously [38,39]. However, it has been proven to also potentiate the signaling of PPARα or PPARδ in mice [40,41], and PPARδ activation is deeply involved in the prevention of body weight gain by telmisartan [42].

Androgen deprivation therapy remains the gold standard first-line treatment for prostate cancer; however, most tumors gradually acquire a castration-resistant phenotype. Several signal pathways responsible for the pathogenesis of CRPC have been elucidated, and growth and survival of CRPC continue to depend on a functional AR signal pathway that is adapted to a microenvironment of low androgen levels [43,44]. At present, several agents targeting AR signaling have been developed, such as a new type of anti-androgens, CYP17 inhibitors, HSP90 inhibitors, histone deacetylase inhibitors, and tyrosine kinase inhibitors [45]. The present data suggest that ARBs are also candidates for suppressor drugs of the AR signal pathway by attenuating AR-mediated transcriptional activity.

Our previous report indicated that ARBs have the potential to decrease or stabilize PSA level of patients with CRPC and inhibit the occurrence of symptoms such as bone pain [9]. These effects seemed to be due to the anti-inflammatory and anti-angiogenesis activity of ARB. In this study, we examined whether ARBs could clinically affect the growth of hormone-naïve cancer cells. In general, it has been reported that aPSA-DT was longer than ePSA-DT from the nadir of biochemical failure (BCF), PSA 0.2 ng/ml [46]. However, olmesartan treatment markedly prolonged PSA-DT in patients with BCF, that is, PSA >0.2 ng/ml after RP, in comparison with non-treated patients (control patients). It is well known that PSA-DT after RP is strongly associated with the risk of cause-specific mortality [47], and is a predictor of development of metastasis [48–50]. In the present study, administration of olmesartan prolonged aPSA-DT 2 fold compared with non-treated patients. These clinical data are consistent with in vivo and in vitro data showing that ARBs have the property to suppress the progression of prostate cancer associated with PSA decrease.

Interspecies scaling is commonly used to extrapolate doses from animal experiments to humans. It is known that plasma concentrations are better than dose levels for the interpretation of animal studies. An approximately five times higher dose in rats compared with human dose level is necessary to reach similar average steady-state plasma levels [51]. Moreover, the 0.75 power of body weight method is conventionally used in scaling [52,53]. The formula is (mg dose in rat)/(rat body weight)$^{3/4}$ = (mg dose in human)/(human body weight)$^{3/4}$, and this can be rewritten as (mg/kg/day dose in rat) × (rat body weight)$^{1/4}$ = (mg/kg/day dose in human) × (human body weight)$^{1/4}$. Applying this formula in the present

experiments using TRAP rats, an equivalent dose of ARBs in human (mg/kg/day) = (10 mg/kg/day) × $(0.3\ kg)^{1/4}/(70\ kg)^{1/4}$ = 2.56 mg/kg/day. This value is equivalent to an intake 2–4 times higher for telmisartan or 14–22 times higher for candesartan than the respective standard intake level in a 70 kg-sized person. In practical terms, however, candesartan is effective for suppressing serum PSA levels at a dose within 4–8 mg/day in advanced prostate cancer patients [9,10]. Therefore, a normal dose of ARBs used in the clinical scenario should provide satisfactory responses of human prostate cancers.

In conclusion, ARBs impede prostate cancer progression by affecting AR expression. These data may contribute to the establishment of a novel chemopreventive and alternative chemotherapeutic strategy for human prostate cancer.

ACKNOWLEDGMENTS

This work was supported by a Grant-in-Aid for the 3rd Term Comprehensive 10-Year Strategy for Cancer Control from the Ministry of Health, Labour and Welfare of Japan and a grant from the Society for Promotion of Pathology of Nagoya, Japan. This work was also supported by a Grant-in-Aid for Scientific Research from the Ministry of Education, Culture, Science and Technology of Japan, and a grant from the Umehara Foundation of Yokohama Medical Group.

REFERENCES

1. Siegel R, Ward E, Brawley O, Jemal A. Cancer statistics, 2011. The impact of eliminating socioeconomic and racial disparities on premature cancer deaths. CA Cancer J Clin 2011;61:212–236.
2. Franceschi S, La Vecchia C. Cancer epidemiology in the elderly. Crit Rev Oncol Hematol 2001;39:216–226.
3. Cunha GR, Donjacour AA, Cooks PS, Mee S, Bigsby RM, Higgins SJ, Sugimura Y. The endocrinology and developmental biology of the prostate. Endocr Rev 1987;8:338–362.
4. Denis LJ, Griffiths K. Endocrine treatment in prostate cancer. Semin Surg Oncol 2000;18:52–74.
5. Ager EI, Neo J, Christophi C. The renin-angiotensin system and malignancy. Carcinogenesis 2008;29:1675–1684.
6. Hunyady L, Catt KJ. Pleiotropic AT1 receptor signaling pathways mediating physiological and pathogenic actions of angiotensin II. Mol Endocrinol 2006;20:953–970.
7. Nahmias C, Strosberg D. The angiotensin AT2 receptor: searching for signal-transduction pathways and physiological function. Trends Pharmacol Sci 1995;16:223–225.
8. Smith GR, Missailidis S. Cancer, inflammation and the AT1 and AT2 receptors. J Inflamm 2004;1:3.
9. Uemura H, Hasumi H, Kawahara T, Sugiura S, Miyoshi Y, Nakaigawa N, Teranishi J, Noguchi K, Ishiguro H, Kubota Y. Pilot study of angiotensin II receptor blocker in advanced hormone-refractory prostate cancer. Int J Clin Oncol 2005;10:405–410.
10. Yamagishi T, Uemura H, Nakaigawa N, Noguchi K, Kubota Y. Angiotensin II blocker decreases serum prostate specific antigen in hormone refractory prostate cancer. J Urol 2005;173:441.
11. Uemura H, Hasumi H, Ishiguro H, Teranishi J, Miyoshi Y, Kubota Y. Renin-angiotensin system is an important factor in hormone refractory prostate cancer. Prostate 2006;66:822–830.
12. Asamoto M, Hokaiwado N, Cho YM, Takahashi S, Ikeda Y, Imaida K, Shirai T. Prostate carcinomas developing in transgenic rats with SV40 T antigen expression under probasin promoter control are strictly androgen dependent. Cancer Res 2001;61:4693–4700.
13. Cho YM, Takahashi S, Asamoto M, Suzuki S, Inaguma S, Hokaiwado N, Shirai T. Age-dependent histopathological findings in the prostate of probasin/SV40 T antigen transgenic rats. Lack of influence of carcinogen or testosterone treatment. Cancer Sci 2003;94:153–157.
14. Seeni A, Takahashi S, Takeshita K, Tang M, Sugiura S, Sato S, Shirai T. Suppression of prostate cancer growth by resveratrol in the transgenic rat for adenocarcinoma of prostate (TRAP) model. Asian Pacific J Cancer Prev 2008;9:7–14.
15. Takahashi S, Takeshita K, Seeni A, Sugiura S, Tang M, Sato S, Kuriyama H, Nakadate M, Abe K, Maeno Y, Nagao M, Shirai T. Suppression of prostate cancer in a transgenic rat model via gamma-tocopherol activation of caspase signaling. Prostate 2009;69:644–651.
16. Kosaka T, Miyajima A, Takayama E, Kikuchi E, Nakashima J, Ohigashi T, Asano T, Sakamoto M, Okita H, Murai M, Hayakawa M. Angiotensin II type I receptor antagonist as an angiogenic inhibitor in prostate cancer. Prostate 2007;67(1):41–49.
17. Sporn MB. Approaches to prevention of epithelial cancer during the preneoplastic period. Cancer Res 1976;36:2699–2702.
18. Parkin DM, Bray FI, Devesa SS. Cancer burden in the year 2000. The global picture. Eur J Cancer 2001;37(Suppl 8):S4–S66.
19. Gronberg H. Prostate cancer epidemiology. Lancet 2003;361(9360):859–864.
20. Nelson WG, De Marzo AM, Isaacs WB. Prostate cancer. N Engl J Med 2003;349:366–381.
21. Gupta S. Prostate cancer chemoprevention: Current status and future prospects. Toxicol Appl Pharmacol 2007;224:369–376.
22. Nelson PS, Montgomery B. Unconventional therapy for prostate cancer: Good, bad or questionable? Nature Rev Cancer 2003;3:845–858.
23. Lippman SM, Klein EA, Goodman PJ, Lucia MS, Thompson IM, Ford LG, Parnes HL, Minasian LM, Gaziano JM, Hartline JA, Parsons JK, Bearden JD, Crawford ED, Goodman GE, Claudio J, Winquist E, Cook ED, Karp DD, Walther P, Lieber MM, Kristal AR, Darke AK, Arnold KB, Ganz PA, Santella RM, Albanes D, Taylor PR, Probstfield JL, Jagpal TJ, Crowley JJ, Meyskens FL Jr, Baker LH. Coltman CA Jr. Effect of selenium and vitamin E on risk of prostate cancer and other cancers. JAMA 2009;301:39–51.
24. Thompson IM, Tangen CM, Goodman PJ, Lucia MS, Klein EA. Chemoprevention of prostate cancer. J Urol 2009;182:499–507.
25. Andriole GL, Bostwick DG, Brawley OW, Gomella LG, Marberger M, Montorsi F, Pettaway CA, Tammela T, Teloken C, Tindall DJ, Somerville MC, Wilson TH, Fowler IL, Rittmaster RS, Group RS. Effect of dutasteride on the risk of prostate cancer. N Engl J Med 2010;362:1192–1202.

26. Dusing R. Effect of the angiotensin II antagonist valsartan on sexual function in hypretensive men. Blood Press Suppl 2003; 2:29–34.
27. Nomura M, Nishii H, Ozaki Y, Fujimoto N, Matsumoto T. An angiotensin II receptor blocker increases sexual behavior in type 2 diabetic mice. Physiol Behav 2007;91:223–228.
28. Yang R, Yang B, EWen Y, Fang F, Cui S, Lin G, Sun Z, Wang R, Dai Y. Losartan, an angiotensin type I receptor, restores erectile function by downregulation of cavernous renin-angiotensin system in streptozocin-induced diabetic rats. J Sex Med 2009; 6:696–707.
29. Cho YM, Takahashi S, Asamoto M, Suzuki S, Tang M, Shirai T. Suppressive effects of antiandrogens, finasteride and flutamide on development of prostatic lesions in a transgenic rat model. Prostate Cancer Prostatic Dis 2007;10:378–383.
30. Tang M, Ogawa K, Asamoto M, Hokaiwado N, Seeni A, Suzuki S, Takahashi S, Tanaka T, Ichikawa K, Shirai T. Protective effects of citrus nobiletin and auraptene in transgenic rats developing adenocarcinoma of the prostate (TRAP) and human prostate carcinoma cells. Cancer Sci 2007;98:471–477.
31. Weihua Z, Mäkelä S, Andersson LC, Salmi S, Saji S, Webster JI, Jensen EV, Nilsson S, Warner M. Gustafsson J-Å. A role for estrogen receptor β in the regulation of growth of the ventral prostate. Proc Natl Acad Sci USA 2001;98:6330–6335.
32. Kato K, Takahashi S, Cui L, Toda T, Suzuki S, Futakuchi M, Sugiura S, Shirai T. Suppressive effects of dietary genistin and daidzin on rat prostate carcinogenesis. Jpn J Cancer Res 2000;91:786–791.
33. Escande A, Pillon A, Servant N, Cravedi J-P, Larrea F, Muhn P, Nicolas J-C, Cavailles V, Balaguer P. Evaluation of ligand selectivity using reporter cell lines stably expressing estrogen receptor alpha or beta. Biochem Pharmacol 2006;71:1459–1469.
34. Comitato R, Nesaretnam K, Leoni G, Ambra R, Canali R, Bolli A, Marino M, Virgili F. A novel mechanism of natural vitamin E tocotrienol activity: Involvement of ERβ signal transduction. Am J Physiol Endocrinol Metab 2009;297:E427–E437.
35. Mak P, Leav I, Pursell B, Bae D, Yang X, Taglienti CA, Gouvin LM, Sharma VM, Mercurio AM. ERbeta impedes prostate cancer EMT by destabilizing HIF-1alpha and inhibiting VEGF-mediated snail nuclear localization: Inplications for Gleason grading. Cancer Cell 2010;17:319–332.
36. Kurtz TW, Pravenec M. Antidiabetic mechanisms of angiotensin-converting enzyme inhibitors and angiotensin II receptor antagonists: Beyond the renin-angiotensin system. J Hypertens 2004;22:2253–2261.
37. Agata J, Ura N, Yoshida H, Shinshi Y, Sasaki H, Hyakkoku M, Taniguchi S, Shimamoto K. Olmesartan is an angiotensin II receptor blocker with an inhibitory effect on angiotensin-converting enzyme. Hypertens Res 2006;29:865–874.
38. Sugimoto K, Qi NR, Kazdova L, Pravenec M, Ogihara T, Kurtz TW. Telmisartan but not valsartan increases caloric expenditure and protects against weight gain and hepatic steatosis. Hypertension 2006;47:1003–1009.
39. Araki K, Masaki T, Katsuragi I, Tanaka K, Kakuma T, Yoshimatsu H. Telmisartan prevents obesity and increases the expression of uncoupling protein 1 in diet-induced obese mice. Hypertension 2006;48:51–57.
40. Clemenz M, Frost N, Schupp M, Caron S, Foryst-Ludwig A, Bohm C, Hartge M, Gust R, Staels B, Unger T, Kintscher U. Liver-specific peroxisome proliferator-activated receptor alpha target gene regulation by the angiotensin type 1 receptor blocker telmisartan. Diabetes 2008;57:1405–1413.
41. He H, Yang D, Ma L, Luo Z, Ma S, Feng X, Cao T, Yan Z, Liu D, Tepel M, Zhu Z. Telmisartan prevents weight gain and obesity through activation of peroxisome proliferator-activated receptor-delta-dependent pathways. Hypertension 2010;55: 869–879.
42. Fleshner N, Fair WR, Huryk R, Heston WDW. Vitamin E inhibit the high-fat diet promoted growth of established human prostate LNCaP tumors in nude mice. J Urol 1999;161:1651–1654.
43. Attar RM, Takimoto CH, Gottardis MM. Castration-resistant prostate cancer: Locking up the molecular escape routes. Clin Cancer Res 2009;15(10):3251–3255.
44. Bonkhoff H, Berges R. From pathogenesis to prevention of castration resistant prostate cancer. Prostate 2010;70:100–112.
45. Chen Y, Sawyers CL, Scher HI. Targeting the androgen receptor pathway in prostate cancer. Curr Opin Pharmacol 2008;8: 440–448.
46. Teeter AE, Presti JCJ, Aronson WJ, Terris MK, Kane CJ, Amling CL, Freedland SJ. Does early prostate-specific antigen doubling time (ePSADT) after radical prostatectomy, calculated using PSA values from the first detectable until the first recurrence value, correlate with standard PSADT? A report from the Shared Equal Access Regional Cancer Hospital Database Group. BJU Int 2009;104:1604–1609.
47. Freedland SJ, Humphreys EB, Mangold LA, Eisenberger M, Dorey FJ, Walsh PC, Partin AW. Death in patients with recurrent prostate cancer after radical prostatectomy: Prostate-specific antigen doubling time subgroups and their associated contributions to all-cause mortality. J Clin Oncol 2007;25:1765–1771.
48. Ponud CR, Partin AW, Eisenberger M, Chan DW, Pearson JD, Walsh PC. Natural history of progression after PSA elevation following radical prostatectomy. JAMA 1999;281:1591–1597.
49. Stewart AJ, Scher HI, Chen MH, McLeod DG, Carroll PR, Moul JW, D'Amico AV. Prostate-specific antigen nadir and cancer-specific mortality following hormonal therapy for prostate-specific antigen failure. J Clin Oncol 2005;23:6556–6560.
50. Ward JF, Zincke H, Bergstralh EJ, Slezak JM, Blute ML. Prostate specific antigen doubling time subsequent to radical prostatectomy as a prognosticator of outcome following salvage radiotherapy. J Urol 2004;172:2244–2248.
51. Ings RMJ. Interspecies scaling and comparisons in drug development and toxicokinetics. Xenobiotica 1990;20:1201–1231.
52. Travis CC, White RK. Interspecific scaling of toxicity data. Risk Anal 1988;8:119–125.
53. Rhomberg LR, Lewandowski TA. Methods for identifying a default cross-species scaling factor. http://www.epagov/raf/publications/pdfs/RHOMBERGSPAPERPDF. 2004.

Cancer Science
The official journal of the Japanese Cancer Association

Purple corn color inhibition of prostate carcinogenesis by targeting cell growth pathways

Ne Long,[1] Shugo Suzuki,[1] Shinya Sato,[1] Aya Naiki-Ito,[1] Keisuke Sakatani,[2] Tomoyuki Shirai[1,3] and Satoru Takahashi[1,4]

[1]Department of Experimental Pathology and Tumor Biology, Nagoya City University Graduate School of Medical Sciences, Nagoya; [2]Food Color Laboratory, San-Ei Gen F.F.I., Inc., Osaka; [3]Nagoya City Rehabilitation Center, Nagoya, Japan

(Received September 24, 2012/Revised November 5, 2012/Accepted November 20, 2012/Accepted manuscript online November 30, 2012/Article first published online January 20, 2013)

Purple corn color is a widely used food colorant that was reported to have attenuating effects on hypertension, diabetes, and to have anti-cancer effects on colon and breast cancer. Our study is the first on its possible chemoprevention effects against prostate cancer. For this purpose an androgen-dependent prostate cancer cell line, LNCaP, was used to examine effects *in vitro*. Purple corn color inhibited the proliferation of LNCaP cells by decreasing the expression of Cyclin D1 and inhibiting the G1 stage of the cell cycle. Thirty-six male transgenic rats for adenocarcinoma of prostate were fed basic diet or diet with purple corn color for 8 weeks. Purple corn color decreased the incidence of adenocarcinoma in the lateral prostate and slowed down the progression of prostate cancer. A lower Ki67 positive rate, a decrease of the expression of Cyclin D1, and downregulation of the activation of Erk1/2 and p38 MAPK were observed in the group consuming purple corn color in the diet. Since purple corn color is a mixture, determining its active component should help in the understanding and usage of purple corn color for prostate cancer chemoprevention. Therefore, the three major anthocyanins in purple corn color, cyanidin-3-glucoside, pelargonidin-3-glucoside and peonidin-3-glucoside, were tested with LNCaP cells. The results suggested that cyanidin-3-glucoside and pelargonidin-3-glucoside are the active compounds. (*Cancer Sci* 2013; 104: 298–303)

Cancer is a major public health problem in developed and some developing countries. In 2012, prostate cancer (PCa) was estimated to be the No.1 cause of new cancer cases in males and the second highest cause of cancer related deaths in the USA,[1] and PCa is rapidly increasing in Asia. Although considerable effort has been expended on searching for early screening markers and curing PCa, the main treatment remains androgen ablation therapy, which was developed in the early 1940s.[2,3] However, even though more than 80% of PCa respond to this therapy, almost all of these cases relapse in less than a decade and become refractory to treatment.[3] Brachytherapy, radiotherapy, and prostatectomy of PCa prior to metastasis can affect a cure, but these procedures can dramatically alter the quality-of-life of the patient.[4,5] Therefore, prevention of PCa is especially important.

The field of chemoprevention, using natural or laboratory-made substances to prevent cancer, has become increasingly studied in recent years. Researchers have investigated numerous chemicals that may have chemopreventive effects on PCa *in vitro* and *in vivo*. Three large-scale randomized, controlled clinical trials have been conducted: the SELECT trial found that neither selenium nor Vitamin E reduced the risk of PCa in healthy men at average risk;[6] the PCPT trial found that finasteride, a 5α-reductase inhibitor, reduced the risk of PCa of Gleason 6 or less, whereas there was an increased risk of high grade disease with Gleason 7 or more;[7] the REDUCE trial also encountered similar difficulties with dutasteride, another 5 α-reductase inhibitor.[8] Therefore, the search for an appropriate chemopreventor for PCa needs to be continued.

Purple corn has a long history as a food product. Nowadays its color is widely used as a food colorant in Japan. Previous studies have provided evidence that purple corn color (PCC) has anti-cancer effects on colon and breast cancer.[9,10] It also has attenuating effects on some life style diseases, for example, hypertension, hyperglycemia, and diabetes.[11,12] The present study was conducted as an initial investigation on PCC's effects on PCa. As a result we found that PCC inhibited the proliferation of the androgen-dependent cell line LNCaP *in vitro* and inhibited prostate carcinogenesis *in vivo* in the Transgenic Rat for Adenocarcinoma of Prostate (TRAP) model. The TRAP rat model, in which expression of the Simian virus 40 T antigen is under control of the probasin gene promoter, was established in our laboratory. These animals develop high-grade prostatic intraepithelial neoplasia (HG-PIN) and well-differentiated adenocarcinomas with high incidence in all prostate lobes at 15 weeks of age, all lesions being completely androgen-dependent.[13,14] The model provides an ideal tool to gain insights into possible mechanisms of PCa prevention in relatively short-term studies.[15–19]

Purple corn color is a mixture, which contains several anthocynins. To determine its active component, the three major anthocyanins in PCC, cyanidin-3-glucoside (C3G), pelargonidin-3-glucoside (Pg3G) and peonidin-3-glucoside (P3G), were tested using LNCaP cells. By comparing the effects of these anthocyanins to the effect of the mixture, we found that C3G and Pg3G are the active compounds.

To our knowledge, the present study provides the first evidence that PCC inhibits prostate carcinogenesis in a rat model closely mimicking the human disease. The clues obtained as to the molecular basis of action are of critical importance as first steps towards human clinical trials.

Materials and Methods

Chemicals, reagents, plasmids and cell line. Purple corn color was provided by San-Ei Gen F.F.I. (Osaka, Japan). Lot No. 100413, anthocyanin concentration 12.5% was used for the *in vitro* study. Lot No. 110418, anthocyanin concentration 20.9% was used for the *in vivo* study. C3G (Cyanidin-3-O-glucoside chloride) and P3G (Peonidin-3-O-glucoside chloride) were purchased from Tokiwa Phytochemical (Chiba, Japan). Pg3G (Pelargonidin-3-O-glucoside chloride) was purchased from Extrasynthese (Genay Cedex, France). The chemical structures of C3G, P3G and Pg3G are shown in Supplementary

[4]To whom correspondence should be addressed.
E-mail: sattak@med.nagoya-cu.ac.jp

doi: 10.1111/cas.12078

Figure S1. The LNCaP human PCa cell line (androgen-dependent) was from the American Type Culture Collection (Manassas, VA, USA). The pGL3-PSA luciferase expression vector (pGL3/PSA-Luc) was donated by Dr Chawnshang Chang, University of Rochester Medical Center.

Animals. Male heterozygous TRAP rats with a Sprague–Dawley genetic background were used in the present study. They housed three animals per cage on wood-chip bedding in an air-conditioned animal room at 23 ± 2°C and 50 ± 10% humidity. Food and tap water were available *ad libitum*. The Institutional Animal Care and Use Committees of the Nagoya City University (Nagoya, Japan) specifically approved this study.

Experimental protocol. A total of 36 heterozygous male TRAP rats at 6 weeks of age were randomly divided into three groups. Rats in the control group (n = 13) received powdered basal diet (Oriental MF, Oriental Yeast, Tokyo, Japan). The rats in the other two groups received 0.1% (n = 12) or 1% PCC (n = 11) in the diet for 8 weeks. At the end of week 8, the rats were killed under deep anesthesia. Each prostate was removed and halves of the ventral and lateral lobes were immediately frozen in liquid nitrogen and stored at −80°C until processed; the remaining prostates was fixed in 10% neutral buffered formalin, embedded in paraffin, and sectioned. Testosterone and estrogen levels in the serum were analyzed by radioimmunoassay by SRL (Tokyo, Japan). All experiments were performed under protocols approved by the Institutional Animal Care and Use Committee of Nagoya City University Graduate School of Medical Sciences.

Assessment of prostate neoplastic lesion development. Neoplastic lesions in the prostate glands of TRAP rats were evaluated as previously described.[19] Briefly, neoplastic lesions were classified into three types: low-grade prostatic intraepithelial neoplasia (LG-PIN), HG-PIN and adenocarcinoma. The relative numbers of acini with the histological characteristics of each type, that is, LG-PIN, HG-PIN and adenocarcinoma, were quantified with reference to the total acini in each prostatic lobe.

Immunoblot analysis. The immunoblotting analysis was performed as described previously.[19] Briefly, LNCaP cells or frozen ventral prostate tissues were homogenized in radioimmunoprecipitation assay buffer (150 mM NaCl, 50 mM Tris–HCl [pH 8.0], 1% NP-40, 0.5% sodium deoxycholate, 0.1% SDS, 1 mM phenylmethylsulphonyl fluoride, 1 mM sodium orthovanadate, and protease inhibitor cocktail [Complete, Roche, Mannheim, Germany]) and subjected to immunoblot analysis using standard techniques. The antibodies used were Cyclin D1 and androgen receptor (Santa Cruz Biotechnology, Santa Cruz, CA, USA), cleaved caspase 3, cleaved caspase 7, Erk1/2, phospho-Erk1/2, p38 MAPK and phospho-p38 MAPK (Cell Signaling Technology, Boston, MA, USA), prostate-specific antigen (DAKO, Tokyo, Japan) and β-actin (Sigma-Aldrich, St. Louis, MO, USA). The density of the bands was semi-quantified using ImageJ (version 1.42q, National Institute of Health, Bethesda, MD, USA).

Immunohistochemistry. Deparaffinized sections were incubated with antibodies for Ki-67 (Novocastra Laboratories, Newcastle, UK) and SV40 T antigen (Santa Cruz Biotechnologies). Apoptotic cells in the prostate were detected using an *In Situ* Apoptosis Detection kit (TUNEL method) according to the manufacturer's instructions (Takara Bio, Ohtsu, Japan). Labeling indices were determined as the positive percentage for Ki-67 or TUNEL by randomly picking eight fields of view in the whole ventral/lateral prostate and counting over 1000 prostate epithelial cells under a microscope at high magnification.

Cell proliferation assay. Cell proliferation of LNCaP cells was assessed by manual counting under trypan blue staining. Briefly, LNCaP cells were seeded in 96-well plates at 10 000 cells/well in 200 μL of RPMI media; PCC, C3G, Pg3G or P3G were added 24 h after seeding and the cells were incubated for 72 h; and the cells were removed from the plate with trypsin-EDTA and counted.

RNA extraction, cDNA preparation, and quantitative real-time PCR. Total RNAs of LNCaP cells or frozen prostate tissue was isolated using an RNeasy Mini kit (Qiagen, Valencia, CA, USA) and reverse-transcribed with the Thermoscript first-strand synthesis system (Invitrogen Corporation, Carlsbad, CA, USA). Real-time RT-PCR was performed using Syber Premix Ex Taq II (Takara) in a LightCycler (Roche Diagnostics GmbH). The primers used were: human GAPDH, 60°C, 5′-AACGGATTTGGTCGTATTGG-3′ and 5′-CATACTTCTCATGGTT-CACA-3′; human Cyclin D1, 60°C, 5′-CCGAGAAGCTGTGCATCTAC-3′ and 5′-CAGGTTCAGGCCTTGCACTG-3′; rat GAPDH, 59°C, 5′-GAATGGGAAGCTGGT-CATCA-3′ and 5′-TGGATGCAGGGATGATGTTC-3′; rat probasin, 60°C, 5′-ACTTCCGTCGCATTGAGTGT-3′ and 5′-GTAAACGTCTTGGGATCTCC-3′; rat GK11, 59°C, 5′-GCAGCACCAAACCCCTGGAT-3′ and 5′-TGAGATCTGTCACCTTCTCA-3′.

Cell cycle analysis. LNCaP cells were seeded in 6-well plates at 150 000 cells/well. Purple corn color, C3G or Pg3G were added 24 h after seeding, incubated for 72 h, collected and analyzed with propidium iodide (Guava cell cycle reagent; Guava Technologies, Hayward, CA, USA) according to the Guava Cell Cycle Assay protocol. The cell cycle phase distribution was determined on a Guava PCA Instrument using CytoSoft Software.

Reporter gene assays. LNCaP cells were transfected with the pGL3/PSA-Luc using Nucleofector II. 24 h later, 5 nM DHT and/or PCC were added. After 48 h incubation, the cells were lysed with the buffer supplied in the kit. Luciferase assays were conducted using the dual-luciferase reporter assay system (Promega, Madison, WI, USA), and the phRL-TK vector (Promega) as an internal control, according to the manufacturer's protocol. Data shown are means and SD of four independent data points.

Statistical analysis. All data presented are mean ± SD values. Statistical comparisons were performed with one-way ANOVA followed by Dunnett's test. Correlations were assessed by Spearman correlation coefficient analysis. A P-value of < 0.05 was considered to be significant. All statistical analyses were performed using GraphPad Prism 5 (GraphPad Software, La Jolla, CA, USA).

Results

PCC inhibition of LNCaP proliferation and slowing of the cell cycle. When the androgen-dependent cell line LNCaP was incubated with increasing levels of PCC for 72 h, the proliferation of the cells was inhibited in a dose-dependent manner (Fig. 1A). Cell cycle analysis showed that PCC increased the proportion of cells in G0/G1 slightly but significantly (Fig. 1B). Western blotting showed a 15–30% decrease in the protein level of Cyclin D1 in the PCC treated cells (Fig. 1C), and reverse-transcription PCR also showed that the mRNA level of Cyclin D1 was significantly decreased by PCC (Fig. 1D). Purple corn color did not affect androgen receptor (AR) expression, but PSA expression was dramatically decreased (Fig. 1C). Since the PSA gene is a target of AR, we used a luciferase assay to examine the influence of PCC on the activity of the PSA promoter. Purple corn color inhibited functional AR transcriptional activity in a dose-dependent manner (Fig. S2).

No toxic effects of PCC were observed in the TRAP rat model. Body weights, relative organ weights (ventral prostate, liver and kidney), and food consumption were not affected by administration of PCC in the diet to TRAP rats (Table S1). The average PCC intakes were 25 mg/rat per day and 267 mg

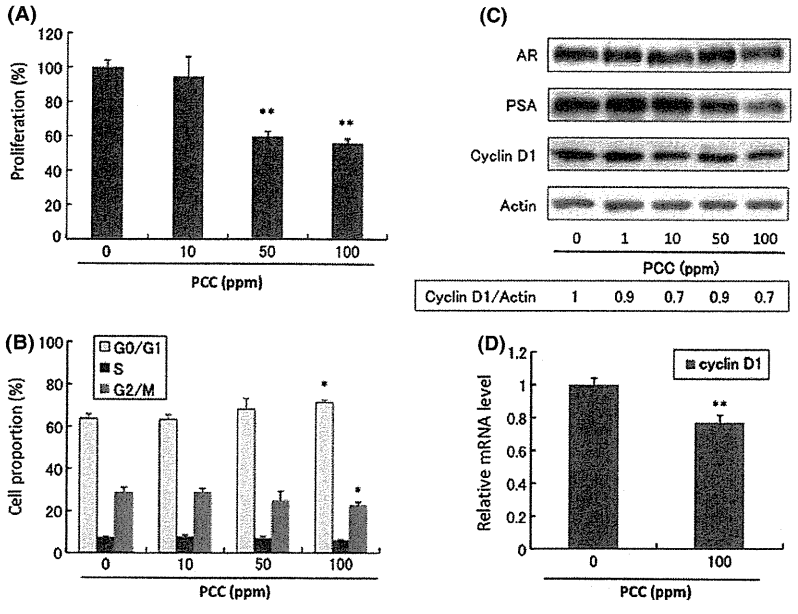

Fig. 1. Effects of purple corn color (PCC) on LNCaP cells. (A) Inhibitory effects on LNCaP cell proliferation (72 h) (n = 3). (B) Effects on the cell cycle of LNCaP cells (n = 3). (C) Protein changes assessed by Western blotting analysis of LNCaP cells after incubation with PCC for 72 h. The density of the bands of Cyclin D1 and actin were semi-quantified by ImageJ. (D) mRNA levels of Cyclin D1 analyzed by reverse-transcription polymerase chain reaction (n = 3). *P < 0.05; **P < 0.01; ***P < 0.001.

/rat per day for the 0.1% and 1% PCC groups (Table S1). Purple corn color did not have any effect on the serum levels of testosterone or estradiol (Table S1).

PCC inhibition of prostate carcinogenesis in the TRAP rat model. With the expression of SV40T antigen under the control of AR, TRAP rats developed prostate cancer with high incidence. In the end of the experiment, all the acini in both ventral and lateral prostate of TRAP rats had developed precancerous or cancerous lesions. Lesions were divided into three stages: LG-PIN, HG-PIN, and adenocarcinoma (Fig. S3). The total percentage of LG-PIN, HG-PIN and adenocarcinoma is 100%. In this study, adenocarcinomas were observed in ventral prostate of all the rats, that is, the incidence of adenocarcinoma was 100% in all three groups. However, the rats consuming PCC had a lower percentage of adenocarcinoma and a higher percentage of LG-PIN (Table 1), which suggests that PCC retarded the progression of PCa and more acini lesions remained in the relatively benign LG-PIN stage. The increased LG-PIN percentage and decreased adenocarcinoma percentage showed a strong correlation to the dose of PCC. In the lateral prostate, we also observed this retardation of PCa progression. Of critical importance in this study is that PCC also significantly decreased the incidence of adenocarcinoma in the lateral prostate (Table 1). These results suggest that PCC inhibited tumorigenesis in the prostates of TRAP rats.

PCC inhibition of the cell growth pathways in the TRAP rat model. Carcinogenesis in the TRAP rat is induced by SV40T antigen expressed under the control of the probasin promoter, which is regulated by the AR. Since PCC downregulated AR activity *in vitro*, we examined whether SV40T expression was downregulated by PCC. Immunohistochemical analysis showed that there was no overt inhibition of SV40T expression by PCC (Fig. 2A,B). We used RT-PCR to examine mRNA levels in the VP of the androgen responsive genes probasin and GK11, an ortholog of human PSA. These results also indicated that AR activity was not inhibited by PCC (Fig. 2C).

Figure 3A shows that the Ki67 index was decreased by PCC in both VP and LP. On the other hand, the TUNEL staining index was not affected by PCC (Fig. 3B), in agreement with our *in vitro* studies in which no apoptosis was observed (data not shown).

Immunoblotting demonstrated factors involved in cell growth pathways, Erk1/2 and p38 MAPK phosphorylation and Cyclin D1, to be downregulated by PCC. In agreement with the results of TUNEL staining, PCC had no affect on the levels of cleaved caspases 3 or 7 (Fig. 3C).

Search for active compounds in PCC. The compounds that give PCC its purple color are anthocyanins. C3G, Pg3G and P3G are the three major components of PCC. When their effects on LNCaP cells were tested, C3G and Pg3G dose-dependently inhibited the proliferation of LNCaP cells, while P3G had no effect (Fig. 4A). The differences of the chemical structures of these three chemicals (Fig. S1) suggest that the hydroxyl radical may play an important role in the inhibitory activity on PCa. Both C3G and Pg3G upregulated AR expression. However, PSA expression, an indicator of AR activity, remained the same (Fig. 4B). This effect on AR activity is in contrast to the effect of PCC *in vitro* but similar to that *in vivo*. Both C3G and Pg3G decreased the expression of Cyclin D1 (Fig. 4C), while increasing the proportion of cells in G0/G1 (Fig. 4D,E), again in line with the PCC effect.

Discussion

Purple corn color is reported to have anti-cancer effect on colon and breast cancer,[9,10] and it also has attenuating effects on some life style diseases, for example, hypertension, hyperglycemia, and diabetes.[11,12] Like breast cancer, PCa is hormone-related. Prostate cancer is also closely associated with a high-fat diet.[20,21] Finally, in the TRAP model, hypertension is positively associated with PCa development.[22] Therefore, we investigated the possibility that PCC could have inhibitory effects on PCa. The results of our experiments, both *in vitro* and *in vivo*, supported this hypothesis. Purple corn color not only showed antiproliferative effects on an androgen-dependent PCa cell line, it also inhibited prostate carcinogenesis *in vivo*. Importantly, dietary PCC did not have any observable toxic effects: there were no significant changes in the final body weights or relative liver or kidney weights in rats fed PCC in their diets. This suggests that PCC could be used as a long-term dietary supplement for chemoprevention of PCa. The success of PCC in the TRAP

doi: 10.1111/cas.12078

Table 1. Quantitative evaluation of neoplastic lesions in prostates of TRAP rats treated with PCC

	No. of animal	Incidence of adenocarcinoma	Proportion of acini in different stages of carcinogenesis (%)		
			LG-PIN	HG-PIN	Adenocarcinoma
Ventral prostate					
Control	13	13 (100%)	4.4 ± 2.8	89.2 ± 3.5	6.4 ± 4.0
0.1% PCC	12	12 (100%)	5.9 ± 3.4**	90.6 ± 3.8	3.5 ± 1.7***
1% PCC	11	11 (100%)	9.1 ± 3.9**	88.2 ± 3.4	2.7 ± 2.0***
Lateral prostate					
Control	13	12 (92%)	24.7 ± 12.4	72.8 ± 11.7	2.5 ± 2.8
0.1% PCC	12	7 (58%)	17.8 ± 5.6	81.2 ± 5.6	1.0 ± 1.0**
1% PCC	11	3 (27%)*	21.1 ± 6.8	78.0 ± 6.2	0.9 ± 1.6**

AC, adenocarcinoma; HG, high grade; LG-PIN, low grade prostatic intraepithelial neoplasia. *$P < 0.01$ versus control (Dunnett's test). **$P < 0.01$ and ***$P < 0.001$ versus control, respectively (Spearman's rank correlation coefficient analysis).

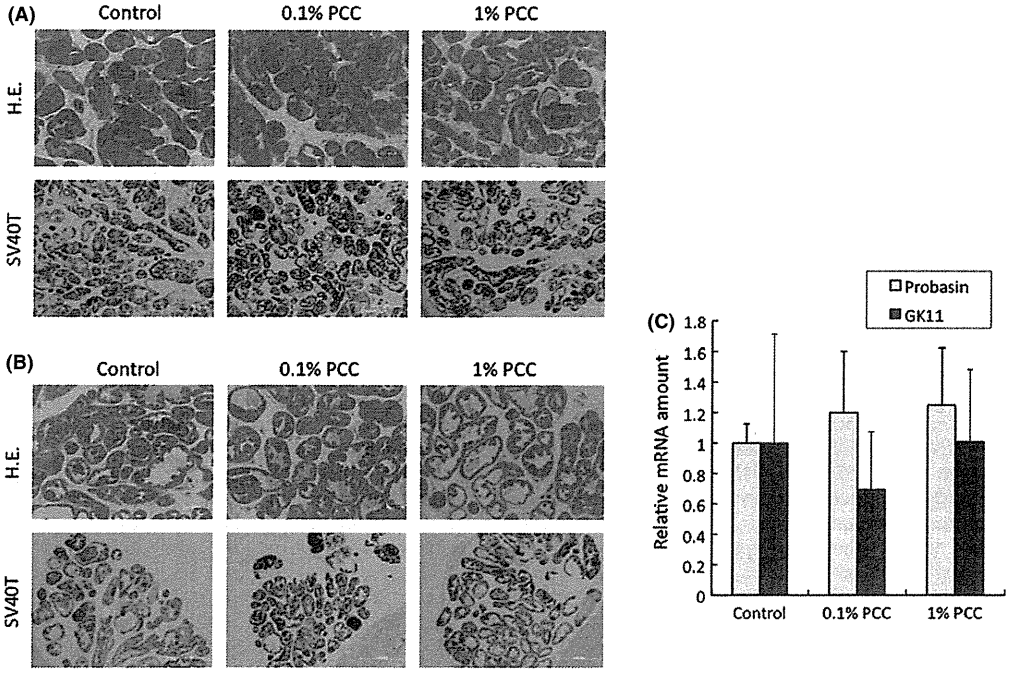

Fig. 2. Purple corn color (PCC)-mediated inhibition of carcinogenesis is not due to down regulation of androgen receptor (AR) activity. (A) H&E staining (4 × magnification) and SV40T antigen expression (4 × magnification) in the ventral prostate. (B) H&E staining (4 × magnification) and SV40T antigen expression (4 × magnification) in the lateral prostate. (C) mRNA of the ventral prostate was used for reverse-transcription polymerase chain reaction. mRNA levels of probasin and GK11 (the rat ortholog of human PSA), which are AR target genes, were checked. Scale bars, 500 μm.

rat model demonstrates that PCC may inhibit prostate carcinogenesis not only in a simple *in vitro* tissue culture system but also in the complex system of living experimental animals.

To date, an enormous effort has been made to find means to prevent PCa, but an ideal chemopreventor active by itself has yet to be found. The trend has therefore been to put chemicals that target different pathways together to form a "cocktail" that would be more effective. Our laboratory has been focused on looking for PCa chemopreventors. We previously reported that resveratrol could inhibit PCa genesis by targeting the AR pathway,[19] while γ-tocopherol exerts inhibitory effects though activation of caspase-signaling.[23] In the present study, we found that PCC targets cell growth. A reasonable expectation is that combining PCC, resveratrol and γ-tocopherol could have a greater effect than using any of the compounds singly. This is a direction for future studies.

To better understand the chemopreventive effects of PCC on PCa, identifying the active components is essential. Cell proliferation assays here indicated that both C3G and Pg3G dose-dependently inhibited the growth of LNCaP. Similarly to PCC, both C3G and Pg3G decreased the expression of Cyclin D1 and increased the percentage of LNCaP cells in G0/G1. The increased percentage of cells in G0/G1 was about 1.1 times compared to the control. Importantly, the cell proliferation was inhibited by approximately 50%. This suggests that while the effect of C3G and Pg3G on the cell proliferation is rather small, the cumulative effect over time can be substantial. Intriguingly, although the PCC mixture downregulated AR activity, C3G and Pg3G did not show the same effect. Notably, PCC inhibited carcinogenesis in the TRAP model without

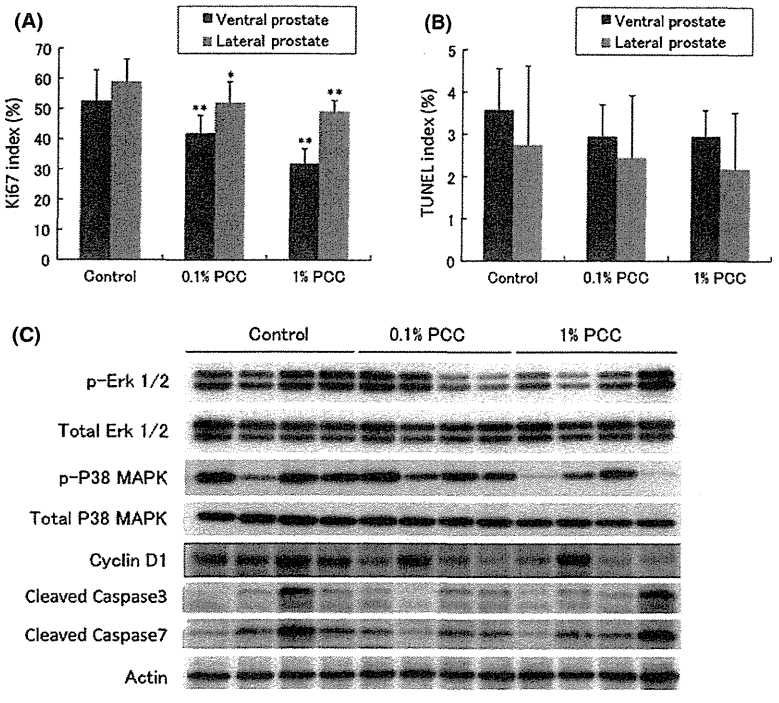

Fig. 3. Effects of purple corn color (PCC) on Ki67 and terminal deoxynucleotidyl transferase-mediated dUTP nick end labeling (TUNEL) indices in the prostate. (A) Purple corn color decreased the Ki67 index significantly in both the ventral and lateral prostate (samples from all the rats were used for analysis). (B) Purple corn color did not affect the TUNEL index in either the ventral or lateral prostate (samples from all the rats were used for analysis). (C) Western blot of proteins related to cell growth and apoptosis using samples from the ventral prostate.

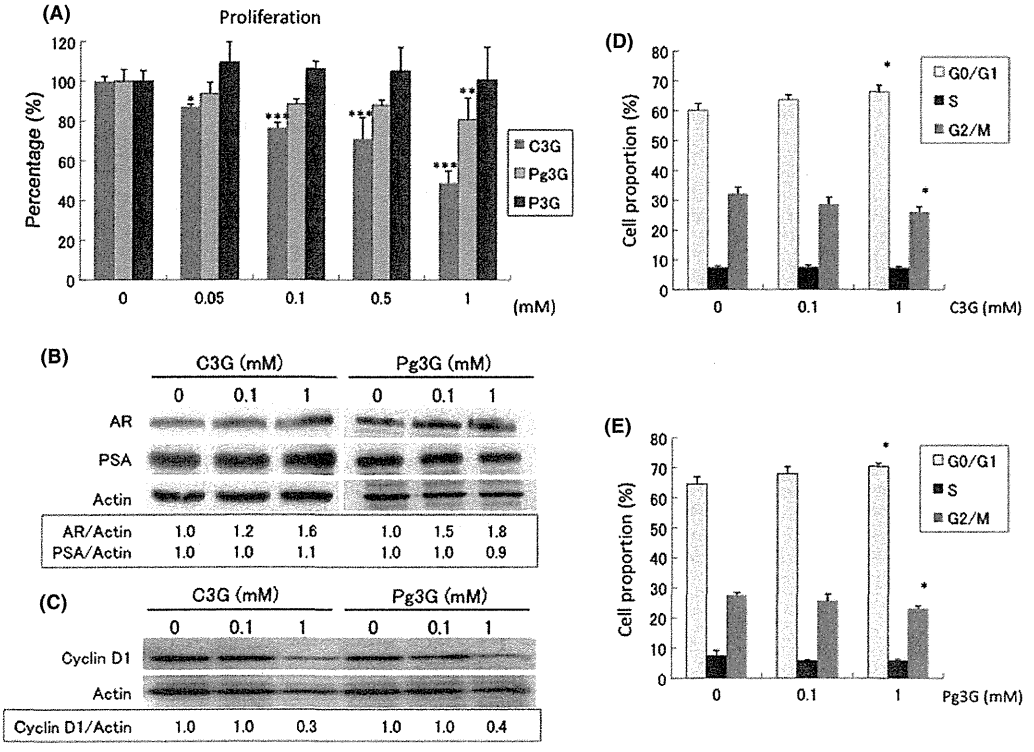

Fig. 4. Anthocyanins in the purple corn color (PCC) mixture, cyanidin-3-glucoside (C3G), pelargonidin-3-glucoside (Pg3G) and peonidin-3-glucoside (P3G), were tested using LNCaP cells. (A) Effects of C3G, Pg3G and P3G on LNCaP cell proliferation. (B,C) Findings of Western blotting. The density of the bands of androgen receptor (AR), PSA and actin were semi-quantified by ImageJ. (D) Effects of C3G on the cell cycle of LNCaP cells. (E) Effects of Pg3G on the cell cycle of LNCaP cells. $*P < 0.05$; $**P < 0.01$; $***P < 0.001$.

downregulating AR activity. Therefore, it is likely that PCC does not inhibit PCa through downregulation of AR. The downregulation observed with the PCC mixture *in vitro* might be a byproduct of other compounds. Taken together, these results suggest that C3G and Pg3G are the probable active compounds contained in PCC.

doi: 10.1111/cas.12078

Carcinogenesis is a complex and long-term progress. Therefore, finding a chemopreventor and using it to inhibit the progression of PCa will be of general benefit. Our study has proved: (i) the safety of relatively long-term PCC consumption; (ii) PCC can inhibit PCa both *in vitro* and *in vivo*, and modulation of cell growth pathways may possibly be involved in suppressive effects of PCC. Other studies have reported that C3G and Pg3G, the active compounds in PCC, have antioxidant and free-radical-scavenging effects, which may protect cells from oxidative damage and reduce the risk of diabetes, cardiovascular diseases and cancer.[24–27] With further study, we can expect to determine whether the mechanism of PCC inhibition of PCa also involves these pathways. Modulation of multiple pathways can increase the chance of PCC effectively preventing PCa in humans. Taking the available information into account, PCC, a widely used food colorant, appears to be a promising chemopreventor for PCa.

Acknowledgments

This work was supported by a Grant-in-Aid for the 3rd Term Comprehensive 10-year Strategy for Cancer Control from the Ministry of Health, Labour and Welfare of Japan and a grant from the Society for Promotion of Pathology of Nagoya, Japan. The authors thank Koji Kato and Junko Takekawa for their technical assistance with immunohistochemistry.

Disclosure Statement

The authors have no conflict of interest.

References

1 Siegel R, Naishadham D, Jemal A. Cancer statistics, 2012. *CA Cancer J Clin* 2012; **62**: 10–29.
2 Huggins C, Hodges CV. The effect of castration, of estrogen and of androgen injection on serum phosphatases in metastatic carcinoma of the prostate. *Cancer Res* 1941; **1**: 293–7.
3 Rubin MA. Targeted therapy of cancer: new roles for pathologists-prostate cancer. *Mod Pathol* 2008; **21**(Suppl. 2): S44–55.
4 Wei JT, Dunn RL, Sandler HM *et al.* Comprehensive comparison of health-related quality of life after contemporary therapies for localized prostate cancer. *J Clin Oncol* 2002; **20**: 557–66.
5 Sanda MG, Dunn RL, Michalski J *et al.* Quality of life and satisfaction with outcome among prostate-cancer survivors. *N Engl J Med* 2008; **358**: 1250–61.
6 Lippman SM, Klein EA, Goodman PJ *et al.* Effect of selenium and vitamin E on risk of prostate cancer and other cancers: the selenium and vitamin E cancer prevention trial (SELECT). *JAMA* 2009; **301**: 39–51.
7 Thompson IM, Tangen CM, Goodman PJ, Lucia MS, Klein EA. Chemoprevention of prostate cancer. *J Urol* 2009; **182**(2): 499–507; discussion 508.
8 Andriole GL, Bostwick DG, Brawley OW *et al.* Effect of dutasteride on the risk of prostate cancer. *N Engl J Med* 2010; **362**: 1192–202.
9 Hagiwara A, Miyashita K, Nakanishi T *et al.* Pronounced inhibition by a natural anthocyanin, purple corn color, of 2-amino-1-methyl-6-phenylimidazo [4,5-b]pyridine (PhIP)-associated colorectal carcinogenesis in male F344 rats pretreated with 1,2-dimethylhydrazine. *Cancer Lett* 2001; **171**: 17–25.
10 Fukamachi K, Imada T, Ohshima Y, Xu J, Tsuda H. Purple corn color suppresses Ras protein level and inhibits 7,12-dimethylbenz[a]anthracene-induced mammary carcinogenesis in the rat. *Cancer Sci* 2008; **99**: 1841–6.
11 Shindo M, Kasai T, Abe A, Kondo Y. Effects of dietary administration of plant-derived anthocyanin-rich colors to spontaneously hypertensive rats. *J Nutr Sci Vitaminol (Tokyo)* 2007; **53**: 90–3.
12 Tsuda T, Horio F, Uchida K, Aoki H, Osawa T. Dietary cyanidin 3-O-beta-D-glucoside-rich purple corn color prevents obesity and ameliorates hyperglycemia in mice. *J Nutr* 2003; **133**: 2125–30.
13 Asamoto M, Hokaiwado N, Cho YM *et al.* Prostate carcinomas developing in transgenic rats with SV40 T antigen expression under probasin promoter control are strictly androgen dependent. *Cancer Res* 2001; **61**: 4693–700.
14 Cho YM, Takahashi S, Asamoto M *et al.* Age-dependent histopathological findings in the prostate of probasin/SV40 T antigen transgenic rats: lack of influence of carcinogen or testosterone treatment. *Cancer Sci* 2003; **94**: 153–7.
15 Zeng Y, Yokohira M, Saoo K *et al.* Inhibition of prostate carcinogenesis in probasin/SV40 T antigen transgenic rats by raloxifene, an antiestrogen with anti-androgen action, but not nimesulide, a selective cyclooxygenase-2 inhibitor. *Carcinogenesis* 2005; **26**: 1109–16.
16 Kandori H, Suzuki S, Asamoto M *et al.* Influence of atrazine administration and reduction of calorie intake on prostate carcinogenesis in probasin/SV40 T antigen transgenic rats. *Cancer Sci* 2005; **96**: 221–6.
17 Said MM, Hokaiwado N, Tang M *et al.* Inhibition of prostate carcinogenesis in probasin/SV40 T antigen transgenic rats by leuprorelin, a luteinizing hormone-releasing hormone agonist. *Cancer Sci* 2006; **97**: 459–67.
18 Tang M, Ogawa K, Asamoto M *et al.* Protective effects of citrus nobiletin and auraptene in transgenic rats developing adenocarcinoma of the prostate (TRAP) and human prostate carcinoma cells. *Cancer Sci* 2007; **98**: 471–7.
19 Seeni A, Takahashi S, Takeshita K *et al.* Suppression of prostate cancer growth by resveratrol in the transgenic rat for adenocarcinoma of prostate (TRAP) model. *Asian Pac J Cancer Prev* 2008; **9**: 7–14.
20 De Nunzio C, Aronson W, Freedland SJ, Giovannucci E, Parsons JK. The correlation between metabolic syndrome and prostatic diseases. *Eur Urol* 2012; **61**: 560–70.
21 Hoda MR, Mohammed N, Theil G, Fischer K, Fornara P. Obesity and prostate cancer: role of adipocytokines and clinical implications. *Urologe A* 2012; **51**: 1253–60.
22 Takeshita K, Takahashi S, Tang M, Seeni A, Asamoto M, Shirai T. Hypertension is positively associated with prostate cancer development in the TRAP transgenic rat model. *Pathol Int* 2011; **61**: 202–9.
23 Takahashi S, Takeshita K, Seeni A *et al.* Suppression of prostate cancer in a transgenic rat model via gamma-tocopherol activation of caspase signaling. *Prostate* 2009; **69**: 644–51.
24 Sun CD, Zhang B, Zhang JK *et al.* Cyanidin-3-glucoside-rich extract from Chinese bayberry fruit protects pancreatic beta cells and ameliorates hyperglycemia in streptozotocin-induced diabetic mice. *J Med Food* 2012; **15**: 288–98.
25 Delazar A, Khodaie L, Afshar J, Nahar L, Sarker SD. Isolation and free-radical-scavenging properties of cyanidin 3-O-glycosides from the fruits of Ribes biebersteinii *Berl. Acta Pharm* 2010; **60**: 1–11.
26 Xu M, Bower KA, Wang S *et al.* Cyanidin-3-glucoside inhibits ethanol-induced invasion of breast cancer cells overexpressing ErbB2. *Mol Cancer* 2010; **9**: 285.
27 Goulas V, Manganaris GA. The effect of postharvest ripening on strawberry bioactive composition and antioxidant potential. *J Sci Food Agric* 2011; **91**: 1907–14.

Supporting Information

Additional Supporting Information may be found in the online version of this article:

Fig. S1. The chemical structures of C3G, Pg3G and P3G.

Fig. S2. PCC down regulated the activity of the PSA promoter.

Fig. S3. The different stages of carcinogenesis in the prostate of TRAP rat.

Table S1. Final body and organ weights, serum hormone levels, and average PCC intake.

Thermotherapy Using Magnetic Cationic Liposomes Powerfully Suppresses Prostate Cancer Bone Metastasis in a Novel Rat Model

Daichi Kobayashi,[1] Noriyasu Kawai,[1]* Shinya Sato,[2] Taku Naiki,[1] Kenji Yamada,[1] Takahiro Yasui,[1] Keiichi Tozawa,[1] Takeshi Kobayashi,[3] Satoru Takahashi,[2] and Kenjiro Kohri[1]

[1]*Department of Nephro-Urology, Nagoya City University Graduate School of Medical Sciences, Mizuho-ku, Nagoya, Japan*

[2]*Department of Experimental Pathology and Tumor Biology, Nagoya City University Graduate School of Medical Sciences, Mizuho-ku, Nagoya, Japan*

[3]*College of Bioscience and Biotechnology, Chubu University, Matsumoto-cho, Kasugai, Japan*

BACKGROUND. Bone metastasis is a serious problem for individuals with prostate cancer, and the effects of the anticancer drug docetaxel (DTX) are insufficient. We therefore examined the therapeutic potential of magnetic cationic liposomes (MCL) in a novel rat model that allows the evaluation of tumor immunity. The effects of MCL thermotherapy were compared with those of DTX as a conventional therapy for the treatment of bone metastatic prostate cancer.

METHODS. Prostate tumor tissues were transplanted into the femurs of model rats divided into four groups: control, MCL, DTX, and MCL + DTX. Tumors were injected with MCL, and alternating magnetic field (AMF) irradiation was performed three times a week. Tumor proliferation and bone destruction were evaluated by proliferating cell nuclear antigen positivity, computed tomography, and CD68-positive cell number, while tumor immunity was evaluated by heat shock protein (HSP) 70 expression and CD8-positive lymphocyte number.

RESULTS. We successfully established a novel femur metastasis model of prostate cancer, and demonstrated that tumor proliferation and bone destruction in the MCL and MCL + DTX groups were significantly suppressed compared with control and DTX groups. MCL thermotherapy concurrently induced necrosis and apoptosis. The expression of HSP70 in the MCL and MCL + DTX groups was also significantly increased, and tumor immunity was enhanced through the induction of CD8-positive lymphocytes.

CONCLUSION. MCL thermotherapy was clearly more effective than DTX in treating bone metastatic prostate cancer. A combination of MCL thermotherapy and DTX therefore deserves consideration as a novel treatment for this disease. *Prostate* © 2013 Wiley Periodicals, Inc.

KEY WORDS: **magnetic cationic liposomes; bone metastasis; cell death; combination therapy; docetaxel; osteoclasts**

INTRODUCTION

Bone metastasis and lymph node metastasis are frequently observed in advanced prostate cancer [1]. Among 1,589 autopsy cases of prostate cancer patients from 1967 to 1995, 35% showed hematogenous metastases, with the most frequent involvement being bone (90%) [2–4]. Bone metastases is therefore one of the most important clinical problems faced by prostate cancer patients.

The bone microenvironment is composed of osteoblasts, osteoclasts, the mineralized bone matrix, and

Grant sponsor: Ministry of Education, Culture, Sports, Science and Technology of Japan; Grant numbers: 21592055; 21790390; Grant sponsor: Nagoya City University; Grant sponsor: Ichihara International Scholarship Foundation; Grant sponsor: Aichi Cancer Research Foundation.

No potential conflicts of interest were disclosed.

*Correspondence to: Noriyasu Kawai, Department of Nephro-Urology, Nagoya City University Graduate School of Medical Sciences, 1 Kawasumi, Mizuho-cho, Mizuho-ku, Nagoya 467-8601, Japan. E-mail: n-kawai@med.nagoya-cu.ac.jp

Received 11 October 2012; Accepted 7 December 2012
DOI 10.1002/pros.22637
Published online in Wiley Online Library (wileyonlinelibrary.com).

many other cell types. It is highly favorable for tumor invasion and growth. Crosstalk between tumor cells and the microenvironment promotes a vicious cycle of tumor growth and bone destruction [5–7], whereby metastatic prostate tumor cells in the bone microenvironment produce cytokines that stimulate osteoclastic bone resorption. This results in the release of growth factors that stimulate tumor cell proliferation from the bone matrix, such as TGF-beta [8,9], insulin-like growth factors [8], and bone morphological proteins [10]. Therefore, a different mechanism of cancer cell proliferation is observed in bone metastatic lesions compared to the primary lesion. Because excessive osteoclast activity plays a central role in the pathophysiology of bone disease at each stage of prostate cancer progression, it is necessary to suppress this activity in order to inhibit the development of bone metastatic lesions.

Highly potent inhibitors of osteoclast-mediated bone resorption such as zoledronic acid and anti-RANKL antibody are capable of suppressing osteoclast activity [11–13]; however, the antitumor activity of these agents remains unconfirmed in prostate cancer. On the other hand, anticancer drugs such as docetaxel (DTX), which has a proven effect on castration-resistant prostate cancer, inhibits the growth of cancer cells but does not suppress the activity of osteoclasts. The effects of cancer drugs on bone metastatic lesions are therefore uncertain, and the inhibition of osteoclast and tumor cell growth in the bone microenvironment can be considered important strategies for the treatment of prostate cancer bone metastases.

Thermotherapy is a promising candidate for cancer therapy that has the potential to suppress both tumor growth and osteolysis in the bone microenvironment [14]. In the clinic, heating with a radiofrequency electric field is the most common method of applying this therapy [15]; however, this may induce localized heating in tumors and unexpected hot spots in normal tissue due to the uneven distribution of electrodes. Such effects may be influenced by factors such as tumor size. In this study, we examined the efficacy of thermotherapy for prostate cancer of the bone microenvironment by using magnetic cationic liposomes (MCLs) irradiated with an alternating magnetic field (AMF) [16]. In this process, known as "MCL thermotherapy," MCLs are injected into the tumor and heated by AMF. This limits the heated area compared with conventional thermotherapy, because irradiation with AMF is carried out at the frequency at which MCLs generate heat, allowing only cancer tissue to be heated [17–19]. Using a rat model that mimics human prostate cancer bone metastasis with respect to tumor stromal interaction, we demonstrated that MCL thermotherapy concomitantly suppressed both prostate cancer cell proliferation and osteoclast osteolysis in the bone microenvironment. It was also confirmed that MCL thermotherapy simultaneously suppressed the activity of osteoclasts and the proliferation of cancer cells [16–18]. These results suggest that MCL thermotherapy may be a very useful tool for the treatment of metastases to bone lesions.

In this study, we established a novel rat metastases model of prostate cancer to evaluate tumor growth, bone destruction, and tumor immunity at the same time. This model possesses tumor–stromal interactions that mimic those of human prostate cancer bone metastasis, exhibits reduced side effects in response to repeated thermotherapy, and represents a model of a deep-site tumor compared with a previous model [16]. We also improved the MCL thermotherapy procedure in this study. First, the injection method was changed. Previously, MCLs were injected into the tumor nodule from one or two sites; however, here, we injected MCLs from four or five different sites around the tumor nodule. Second, we performed AMF irradiation at constant intervals. Previously, treatment had been stopped for 5 days after AMF irradiation because of severe exhaustion of the test rats, and this application of AMF irradiation at inconstant intervals might have been associated with an insufficient therapeutic effect in the previous study. In the present study, we were able to perform irradiation at constant intervals, thereby alleviating rat exhaustion. Finally, we increased the total MCL volume injected in order to treat a deep tumor rather than a subcutaneous tumor. We then used our rat model treated with this improved procedure to test our hypothesis that MCL thermotherapy is superior to DTX as a conventional therapy for the treatment of bone metastatic prostate cancer. In addition to evaluating the efficacy of MCL thermotherapy compared with DTX, we evaluated the effectiveness of combination therapy with both MCL thermotherapy and DTX.

MATERIALS AND METHODS

Animals

Six-week-old male F344 rats were obtained from Charles River, Japan, Inc. (Atsugi, Japan). They were randomly divided into groups of three animals per plastic cage with hard wood chips as bedding in an air-conditioned room at 22% ± 2% and 55% ± 5% humidity, with a 12-hr light/dark cycle. Food (Oriental MF; Oriental Yeast Co., Tokyo, Japan) and tap water were available ad libitum. The research was conducted according to the Guidelines for the Care and Use of Laboratory Animals of Nagoya City University Medical School, and the experimental protocol was

approved by the Institutional Animal Care and Use Committee (H21-M13).

Tumor Tissue

Androgen-independent prostate cancer tissue, PLS-P, was established in the Department of Experimental Oncology and Tumor Biology, Nagoya City University Graduate School of Medical Sciences [20]. This tumor tissue was developed from 3,2-dimethyl-4-aminobiphenyl plus testosterone-induced cancer in the dorsal prostate of male F344 rats. It forms well-differentiated adenocarcinoma with abundant connective tissue stroma, and is immunohistochemically negative for androgen receptor. This tissue can be transplanted into syngenic F344 rats [9,16,21].

Preparation of MCLs

MCLs were fabricated from colloidal magnetite (a kind gift from Toda Kogyo, Hiroshima, Japan) and a lipid mixture consisting of *N*-(a-trimethylammonioacetyl)-didodecyl-D-glutamate chloride (Sogo Pharmaceutical, Tokyo, Japan), dilauroylphosphatidylcholine, and dioleoylphosphatidyl-ethanolamine (Sigma, St. Louis, MO) in a molar ratio of 1:2:2, as described previously [22,23].

Animal Experiment

Approximately 0.5 g aliquots of PLS-P were transplanted into the femur bones of 6-week-old male F344 rats under anesthesia. An incision of approximately 1 cm was made in the skin at the femur and a pocket beneath the skin and muscle was formed using forceps. Prostate tumor tissue was then inserted into the pocket, and the incision was closed using surgical sutures and autoclips (BD Biosciences, Bedford, MA). Body weight was measured every 2 days from the start to the end of therapy. Tumor volume was also measured every 2 days from day 11 to the end of therapy. Tumor diameters were measured in three directions using an external caliper, while tumor volume was calculated using an ellipsoidal formula (tumor volume = 4/3pi(a × b × c), where a, b, and c are the 3 radii) [24,25]. One week after transplantation, autoclips were removed. Three weeks after transplantation, rats were divided into four groups (control group, MCL treatment group, DTX intravenous injection group, MCL + DTX group; number of rats per group, n = 5). The DTX and MCL + DTX groups were administered DTX (10 mg/kg) intravenously on day 0 of this experiment. MCLs (30 mg/ml) were injected directly into the tumors of the MCL and MCL + DTX groups on both the right and left sides in two separate volumes of 0.3 ml (0.6 ml in total) using a Hamilton syringe (Hamilton, Reno, NV) and a syringe pump (KDS, Tokyo, Japan). AMF irradiation was performed three times a week. On day 21 after the start of therapy, all rats were sacrificed and radiography of the transplantation sites was performed with XED-125M (Shimadzu, Tokyo, Japan) and CT (Hitachi Aloka Co. Ltd, Mitaka, Tokyo, Japan). Femur tumors with part of the femur bone were excised en bloc, fixed with 10% buffered formalin solution, and processed for histological examination. For quantitative analysis of bone destruction, the total remaining bone area in hematoxylin and eosin (H & E)-stained sections was examined under a light microscope connected to an image analysis system, including an image processor for analytical pathology (IPAP; Sumika Technos Corp., Osaka, Japan), in order to calculate the remaining bone area. Remaining bone volume was calculated by CT.

AMF Irradiation

An AMF was created using a horizontal coil (inner diameter: 7 cm; length: 7 cm) with a transistor inverter (LTG-100-05; Dai-ichi High Frequency, Tokyo, Japan) operating at 360 kHz. Magnetic field intensity was 30.6 kA/m (384 Oe). Each rat was placed inside the coil such that the tumor nodule was positioned at the center of the coil (Fig. 1A). During AML irradiation, the surface temperature of the rat at the MCL-injected tumor site was locally elevated compared with other surfaces of the rat (Fig. 1B). Temperatures at the center of the tumor and inside the rectum during application of the AMF were measured by an optical fiber probe (FX-9020; Anritsu Meter, Tokyo, Japan) inserted into the tumor and rectum. The temperature at the center of the tumor was maintained at approximately 48–49°C by controlling magnetic field intensity. The temperature at the tumor surface was approximately 35–40°C, while the temperature in the rectum was within the physiological range during AMF irradiation (35–37°C).

Western Blotting

Transplanted prostate tumor tissue, which was partially resected from the tumor and frozen at sacrifice, was homogenized in RIPA buffer (150 mM NaCl, 50 mM Tris–HCl [pH 8.0], 1% NP-40, 0.5% sodium deoxycholate, 0.1% SDS, 1 mM phenylmethylsulfonyl fluoride, 1 mM sodium orthovanadate, and protease inhibitor cocktail [Complete; Roche, France]). Twenty-microgram aliquots of protein were resolved by SDS–PAGE, and separated proteins were transferred to nitrocellulose membranes and incubated with heat shock protein 70 (HSP70; Cell Signaling Technology, Danvers, MA), cleaved caspase 3 (Cell Signaling

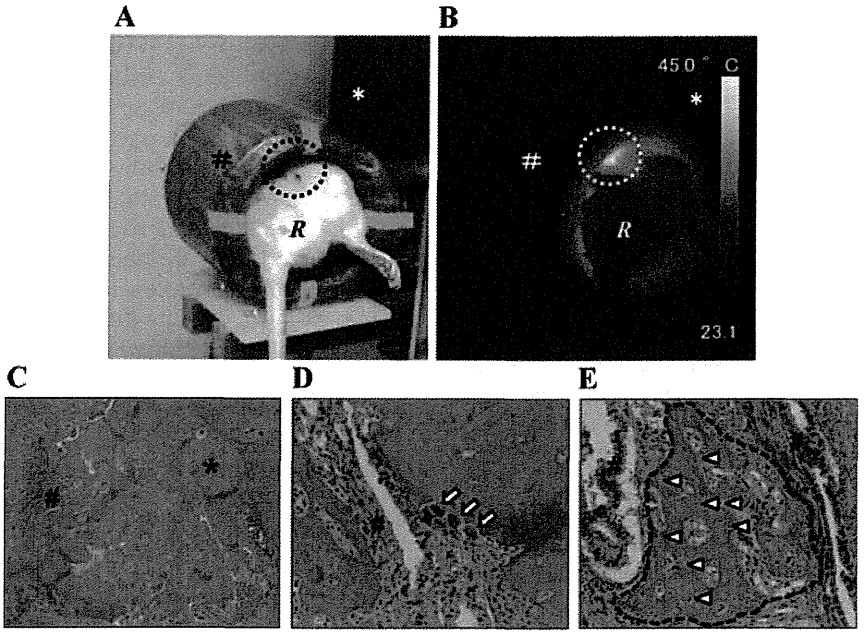

Fig. 1. Tumor-specific hyperthermia measured by thermography and histopathology in a novel rat model of prostate cancer bone metastasis (**A**), Alternating magnetic field (AMF) irradiation machine and rat with magnetic cationic liposomes (MCLs) injected into the transplanted tumor. The rat (R) was placed inside the horizontal coil (#) of the AML irradiation machine (*). The area circled with a dotted line indicates the site of the transplanted tumor injected with MCL. **B**: Tumor-specific hyperthermia measured by thermography. The site of MCL injection was at a high temperature (yellow) compared with the temperature of remainder of the rat (orange). **C**: Hematoxylin and eosin (H & E) staining of transplanted prostate cancer. Prostate cancer cells (#) infiltrated the femur (*; magnification, 20×). **D**: Osteoclasts (arrows) are apparent within the growth of prostate cancer cells (#; magnification, 100×). **E**: Osteoblasts (arrowhead) with osteoid (dotted line) are observed with prostate cancer cells (#) (magnification, 100×).

Technology), interleukin-2 (IL-2; Abcam, Cambridge, UK), interferon-gamma (IFN-gamma) (Abcam), or β-actin (AC-74; Sigma–Aldrich, St. Louis, MO) antibodies. Immunoreactions were visualized with the ECL-Plus detection system (GE Healthcare, Piscataway, NJ) after a 1-hr incubation with horseradish peroxidase-labeled anti-mouse secondary antibodies (Cell Signaling Technology).

Immunohistochemical and Histochemical Analysis

Immunohistochemical staining was applied to paraffin-embedded sections (3 μm thick) of transplanted prostate cancer tissues. Sections were incubated for 60 min with antibodies specific to HSP70, proliferating cell nuclear antigen (PCNA; Dako Cytomation Inc., Glostrup, Denmark), CD68 (AbD Serotec, Kidlington, UK), and CD8a (AbD Serotec). Staining was achieved using two-step EnVision + System-HRP methodology, according to the manufacturer's instructions (Dako Cytomation Inc.). The sections were lightly counterstained with hematoxylin to facilitate orientation. Immunostained slides were evaluated by light microscopy, and the proportion of positively stained cells (positivity) was quantified as positive cancer, normal cell nuclei or membrane/total cancer, and normal cell nuclei or membrane. Berlin blue staining was performed to stain MCL particles.

Statistical Analysis

The significance of the data was determined by Student's *t*-test (two-tailed) using SPSS software (SPSS, Chicago, IL). In vivo analysis was performed using the Mann–Whitney *U*-test of significance. $P < 0.05$ was deemed significant.

RESULTS

Establishment of an Animal Model of Bone Metastatic Prostate Cancer

To assess the anti-cancer effects of repeated thermotherapy in the bone microenvironment, we established a novel rat model that mimics human prostate cancer bone metastasis by transplanting prostate cancer cells into the femur. In the bone

microenvironment of this model, bone destruction (Fig. 1C), as well as osteoclast (Fig. 1D) and osteoblast (Fig. 1E) induction, were observed. The rats showed almost no side effects in response to repeated MCL thermotherapy, such as debilitation or weight loss. While the average body weight of rats in the DTX and MCL + DTX groups was significantly decreased compared with the body weights of rats from the control group from day 7 to day 10, no significant differences in weight were observed among the groups by the end of the experimental period.

MCL Thermotherapy Suppressed Prostate Cancer Growth in the Bone Microenvironment

Tumor volume in the MCL + DTX group was significantly suppressed compared to that in the control and DTX groups (Fig. 2A). Tumor volumes from day 0 to day 11 after therapy showed almost no change in any of the groups. To assess cell proliferation, PCNA immunostaining was performed on specimens of transplanted tumor from each group. Although many cancer cells were positively stained in the control group, only a few cancer cells were positively stained in the MCL and MCL + DTX groups (Fig. 2B), and the percentage of PCNA positively stained cancer cells in these groups was significantly lower than that in the control and DTX groups (Fig. 2C). The percentage of PCNA positively stained cancer cells in the DTX group was almost the same as that in the control group (Fig. 2C).

MCL Thermotherapy Induced Prostate Cancer Necrosis and Apoptosis in the Bone Microenvironment

In order to detect necrotic areas in the tumors, we evaluated tumor necrosis by light microscopy and quantified it using an image analyzer. Necrotic areas were observed in prostate cancer tissue in all groups (Fig. 3A). The necrotic areas in the MCL and MCL + DTX groups extended markedly beyond the MCL-injected area indicated by Berlin blue-positive particles (Fig. 3A). When the necrotic areas were measured quantitatively using the IPAP image analyzer (Fig. 3A, green), the area that was necrotic in the tumors from the MCL and MCL + DTX groups was significantly greater by percentage than that in the control group (Fig. 3B). The percentage of necrotic

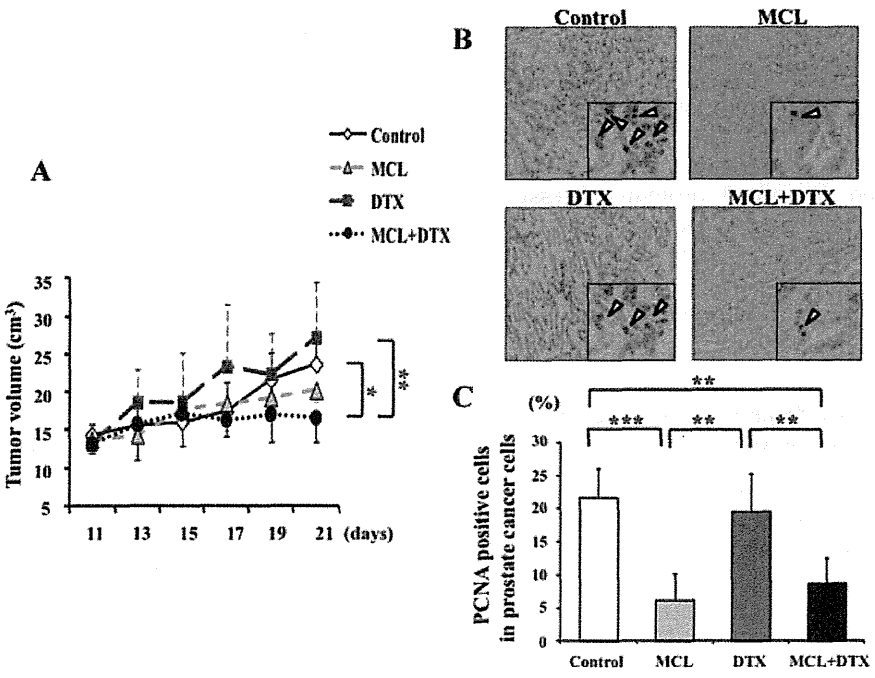

Fig. 2. Tumor growth curve and cell proliferation in a novel rat model of prostate cancer bone metastasis (**A**), sequential changes in transplanted tumor volume (cm^3). Continuous line (◆), dashed spaced line (▲), dashed line (■), and dotted line (●) represent the control group, MCL group, DTX group, and MCL + DTX group, respectively. Values are the mean ± SD ($^*P < 0.05$, $^{**}P < 0.01$). **B**: Immunohistochemistry of PCNA in control, MCL, DTX, and MCL + DTX groups (magnification, 100×; magnification of inclusion photograph, 400×). Positive staining is evident in the nuclei of cancer cells. **C**: PCNA-positive labeling indices. Values are the mean ± SD ($^{**}P < 0.01$, $^{***}P < 0.001$).

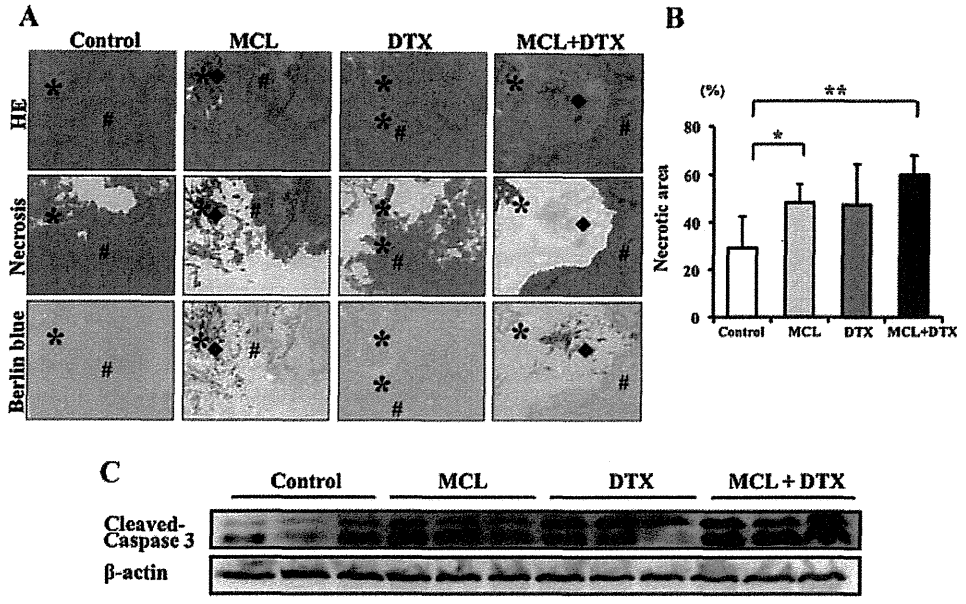

Fig. 3. The evaluation of necrosis and apoptosis in a novel rat model of prostate cancer bone metastasis (**A**), Hematoxylin and eosin (H & E)-stained and Berlin blue-stained tissue sections of transplanted tumors from the control, MCL, DTX, and MCL + DTX groups. Bone (*), MCL (◆), and viable tumor area (#) were noted. Necrotic area was measured with an image analyzer, IPAP (green). In Berlin blue-stained sections, black particles represent MCL particles. (magnification, 20×). **B**: Percentage of necrotic area in the transplanted tumor. Values are the mean ± SD ($^{*}P < 0.05$, $^{**}P < 0.01$). **C**: Cleaved caspase 3 protein expression in transplanted tumors from the control, MCL, DTX, and MCL + DTX groups, as visualized by Western blotting.

area in tumors from the DTX group was also greater than that in the control group, although this difference was not significant (Fig. 3B).

To assess the apoptotic status of the tumor, we evaluated cleaved caspase 3 protein expression in tumors from all four groups. Cleaved caspase 3 expression was observed in the MCL, DTX, and MCL + DTX groups (Fig. 3C), demonstrating that MCL thermotherapy induced necrosis and apoptosis concurrently in the tumors.

MCL Thermotherapy Suppressed Bone Destruction and Osteoclast Induction

Bone destruction is a serious impediment to maintaining the quality of life of patients with bone-metastasized prostate cancer. We examined the effects of MCL and DTX treatment on bone destruction and osteoclast induction in prostate cancer in the bone microenvironment by performing CT and CD68 immunostaining. On CT images, bone destruction was clearly observed in the control group, with less destruction observed in the MCL and MCL + DTX groups (Fig. 4A). Statistically, the remaining bone volume in all treatment groups was greater than that in the control group (Fig. 4B). CD68-positively stained multinuclear cells were also frequently observed in the control and DTX groups, but were scattered in the MCL and MCL + DTX groups (Fig. 4C). When the number of CD68-positive multinuclear cells was determined, tumors from the MCL and MCL + DTX groups were found to have significantly fewer cells than the control and DTX groups (Fig. 4D).

MCL Thermotherapy Induced CD8-Positive Cells, As Well As IL-2, IFN-Gamma, and HSP70 Expression

Previous results have shown that thermotherapy induces tumor immunity. We assessed the induction of tumor immunity in prostate cancer in the bone microenvironment by immunostaining for CD8, which is a marker of cytotoxic T lymphocytes (CTL), the main constituents of tumor immunity. CD8-positive lymphocytes were easily observed in the MCL and MCL + DTX groups compared with the control and DTX groups (Fig. 5A). Statistically, the numbers of CD8-positive lymphocytes in the tumors from the MCL and MCL + DTX groups were significantly increased compared to those in the control and DTX groups (Fig. 5B).

IL-2 and IFN-gamma are known to be cytokines associated with CD8-positive T lymphocytes. We therefore investigated IL-2 and IFN-gamma expression in the tumors by Western blot analysis, and found that

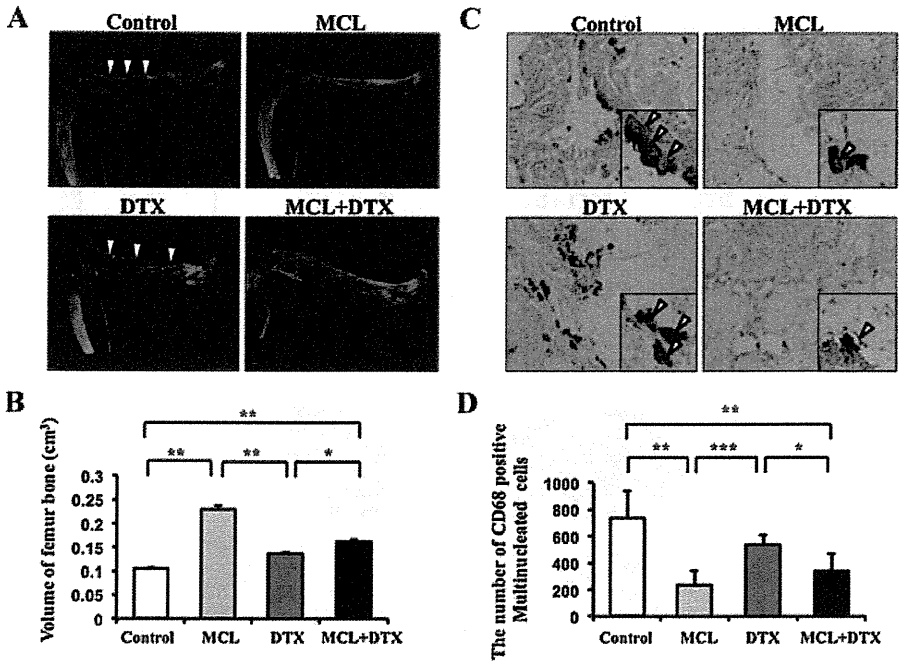

Fig. 4. The evaluation of bone destruction and osteoclast induction in a novel rat model of prostate cancer bone metastasis (**A**), computerized tomography (CT) of rat femur bone with transplanted prostate tumor. The arrowhead indicates destructed femur bone. **B**: Remaining bone volume calculated by CT. Values are the mean ± SD ($^{*}P < 0.05$, $^{**}P < 0.01$). **C**: Immunohistochemistry of CD68 in control, MCL, DTX, and MCL + DTX groups (magnification, 100×; magnification of inclusion photograph, 400×). Positive staining is evident in the cytoplasm and membrane of multinucleated cells. **D**: Number of CD68-positive multinucleated cells of rat femur with transplanted prostate tumor. Values are the mean ± SD ($^{*}P < 0.05$, $^{**}P < 0.01$, $^{***}P < 0.001$).

IL-2 and IFN-gamma protein expression was higher in the tumors from the MCL and MCL + DTX groups than in those from the control and DTX groups (Fig. 5C).

HSP70 is known to be induced by temperature elevation, and to enhance anti-tumor CTL. We therefore investigated HSP70 expression in our model. Using fluorescence immunohistochemistry, HSP70-positive cancer cells were clearly observed in the MCL and MCL + DTX groups, but not in the control and DTX groups. This result was confirmed by Western blot analysis, which showed higher HSP70 protein expression in the tumors from the MCL and MCL + DTX groups than in those from the control and DTX groups (Fig. 5D).

DISCUSSION

Understanding cellular and molecular changes in the bone microenvironment is important for developing novel treatments for prostate cancer bone metastasis. In the bone microenvironment, the growth of metastasized prostate cancer cells is promoted by growth factors secreted to induce bone resorption, which is mediated by osteoclasts [9,26]. Thus, blockade of the vicious cycle between tumor cells and osteoclasts is important for the control of prostate cancer bone metastasis. In this study, we used a novel rat model to examine the efficacy of MCL thermotherapy in the treatment of this disease.

Currently used rodent tumor models, including transgenic tumor models and those in which human tumors are grown subcutaneously in severe combined immunodeficiency (SCID) mice, do not sufficiently represent clinical cancer, especially with regard to metastasis and drug sensitivity. For instance, human prostate cancer cells are commonly transplanted into SCID mice in in vivo experiments examining prostate cancer bone metastasis; however, an investigation into tumor immunity by using such animals is impossible because of their compromised immunocompetence. Rather, the surgical orthotropic transplant (SOI) technique is important in order to obtain clinically accurate models [27,28]. Moreover, a fluorescent SOI model of spontaneous bone metastatic human prostate cancer has previously been reported [29–31]. We therefore employed a novel rat model in this study that maintains normal immunity and allows the evaluation of detailed tumor immunity in vivo, thereby providing an advantage for in vivo investigations. Using this model, we herein demonstrated that

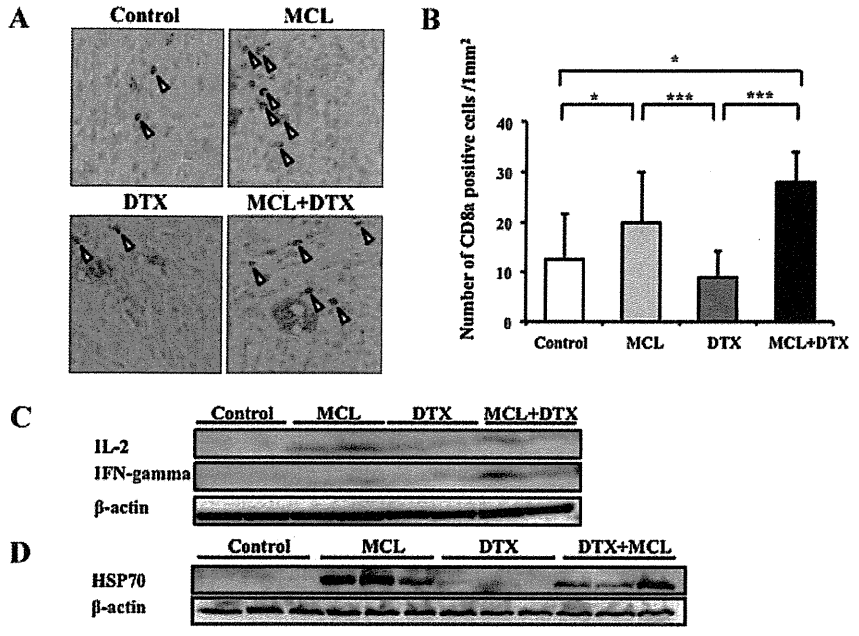

Fig. 5. The evaluation of tumor immunity by the presence of CD8-positive cells and IL-2, IFN-gamma, and HSP70 expression in a novel rat model of prostate cancer bone metastasis (**A**), CD8 immunohistochemistry of the tumor in control, MCL, DTX, and MCL + DTX groups. Positive staining is evident in the nuclei of lymphocytes (magnification, 40 ×). **B**: Number of CD8a-positive cells in the transplanted tumor. Values are the mean ± SD ($^{*}P < 0.05$, $^{***}P < 0.001$). **C**: Western blot analysis of IL-2 and IFN-gamma expression in transplanted tumors from the control, MCL, DTX, and MCL + DTX groups. **D**: Western blot analysis of HSP70 expression in transplanted tumors from the control, MCL, DTX, and MCL + DTX groups.

MCL thermotherapy in this rat model of prostate cancer bone metastasis induced tumor necrosis and apoptosis, suppressed bone destruction and osteoclast induction, and enhanced tumor immunity against prostate cancer in the bone microenvironment. Moreover, we demonstrated that therapy with MCL in conjunction with DTX significantly inhibited tumor growth. Indeed, when cancer cell death was examined, the area of tumor necrosis was found to be significantly greater in both the MCL and MCL + DTX groups than in the control group. Moreover, the induction of apoptosis was observed in tumors from the MCL, DTX, and MCL + DTX groups. These results demonstrate that combination therapy using MCL thermotherapy and DTX can powerfully induce prostate cancer cell death through the activation of different mechanisms.

Thermotherapy has been demonstrated to induce tumor immunity [32], including in a study that found that tumor immunity is induced by MCL thermotherapy in rat glioma [33]. It has been reported that increased HSP70 expression plays a role in the induction of CTL-mediated tumor immunity [34]. In detail, the uptake of HSP70-binding tumor peptide by MHC class I molecules on tumor cells induces the activation tumor-specific CD8-positive T lymphocytes, which are the major immune cells involved in tumor immunity [35,36]. Moreover, after cell death, HSP70-binding tumor peptide is released and engulfed by antigen-presenting cells such as macrophages, which is thought to further induce CD4-positive T lymphocytes. Although HSP70 is believed to be an exacerbation factor under hyperthermia that protects against apoptosis [37–39], and several previous reports have demonstrated that HSP expression induces heat tolerance in cells and adversely affects thermotherapy [40], MCL thermotherapy did not inhibit apoptosis resulting from DTX treatment in this study (Fig. 3C). This suggests that the induction of apoptosis by DTX might be maintained in combination therapy including both MCL and DTX. In addition to the increased number of CD8-positive cells and increased HSP70 protein expression observed in this study, we showed an increase in the expression of IL-2 and IFN-gamma, which are known to induce CD8-positive T lymphocytes. Therefore, we suggest that MCL thermotherapy induces tumor immunity through the up-regulation of HSP70, IL-2, and IFN-gamma, and the subsequent induction of CD8-positive T lymphocytes.

Although the anticancer drug DTX has been proven effective against castration-resistant prostate cancer, DTX induces weight loss as a side effect of